

#### Contents lists available at ScienceDirect

# Petroleum Science





# Original Paper

# Quantitative insight into fracture distribution during supercritical CO<sub>2</sub> fracturing in tight sandstone formation



Bing Yang  $^{a, b, c, *}$ , Hai Huang  $^{b, c, **}$ , Qian-Qian Ren  $^{a, b, c}$ , Hai-Zhu Wang  $^d$ , Bin Wang  $^d$ , Jun Ni  $^e$ , Yong Zheng  $^{b, c}$ , Wen-Tong Zhang  $^f$ 

- <sup>a</sup> The Key Laboratory of Well Stability and Fluid & Rock Mechanics in Oil and Gas Reservoir of Shaanxi Province, Xi'an Shiyou University, Xi'an, 710065, Shaanxi, China
- <sup>b</sup> College of Petroleum Engineering, Xi'an Shiyou University, Xi'an, 710065, Shaanxi, China
- c Shaanxi Key Laboratory of Advanced Stimulation Technology for Oil & Gas Reservoirs, Xi'an Shiyou University, Xi'an, 710065, Shaanxi, China
- <sup>d</sup> State Key Laboratory of Petroleum Resources and Engineering, China University of Petroleum, Beijing, 102249, China
- <sup>e</sup> Shaanxi Yanchang Petroleum (Group) Co., Ltd, Xi'an, 710065, Shaanxi, China
- <sup>f</sup> College of New Energy, Xi'an Shiyou University, Xi'an, 710065, Shaanxi, China

# ARTICLE INFO

#### Article history: Received 21 March 2024 Received in revised form 7 February 2025 Accepted 13 February 2025 Available online 14 February 2025

Edited by Yan-Hua Sun

Keywords: Supercritical CO<sub>2</sub> True-triaxial fracturing Tight sandstone Fracture propagation Ouantitative analysis

#### ABSTRACT

Supercritical CO<sub>2</sub> (SC-CO<sub>2</sub>) fracturing stands out a promising waterless stimulation technique in the development of unconventional resources. While numerous studies have delved into the inducedfracture mechanism of SC-CO<sub>2</sub>, the small scale of rock samples and synthetic materials used in many studies have limited a comprehensive understanding of fracture propagation in unconventional formations. In this study, cubic tight sandstone samples with dimensions of 300 mm were employed to conduct SC-CO<sub>2</sub> fracturing experiments under true-triaxial stress conditions. The spatial morphology and quantitative attributes of fracture induced by water and SC-CO<sub>2</sub> fracturing were compared, while the impact of in-situ stress on fracture propagation was also investigated. The results indicate that the SC-CO<sub>2</sub> fracturing takes approximately ten times longer than water fracturing. Furthermore, under identical stress condition, the breakdown pressure (BP) for SC-CO2 fracturing is nearly 25% lower than that for water fracturing. A quantitative analysis of fracture morphology reveals that water fracturing typically produces relatively simple fracture pattern, with the primary fracture distribution predominantly controlled by bedding planes. In contrast, SC-CO2 fracturing results in a more complex fracture morphology. As the differential of horizontal principal stress increases, the BP for SC-CO<sub>2</sub> fractured rock exhibits a downward trend, and the induced fracture morphology becomes more simplified. Moreover, the presence of abnormal in-situ stress leads to a further increase in the BP for SC-CO2 fracturing, simultaneously enhancing the development of a more conductive fracture network. These findings provide critical insights into the efficiency and behavior of SC-CO<sub>2</sub> fracturing in comparison to traditional water-based fracturing, offering valuable implication for its potential applications in unconventional reservoirs.

© 2025 The Authors. Publishing services by Elsevier B.V. on behalf of KeAi Communications Co. Ltd. This is an open access article under the CC BY-NC-ND license (http://creativecommons.org/licenses/by-nc-nd/

# 4.0/).

# 1. Introduction

As a major energy-consuming country, China is actively promoting the exploration and development of unconventional oil and gas resources that are closely related to national economic

development. Tight sandstone gas, considered an important unconventional resource, has a resource of approximately  $21 \times 10^{12} \, \text{m}^3$  in China. It is primarily distributed in the Paleozoic of the Ordos Basin, the Xujiahe Formation of the Sichuan Basin, the Jurassic of the Turpan-Hami Basin, and the deep layers of Songliao

E-mail addresses: bingyangxsyu@126.com (B. Yang), huanghai@xsyu.edu.cn (H. Huang).

<sup>\*</sup> Corresponding author.

<sup>\*\*</sup> Corresponding author.

and Bohai Bay Basins (Wang and Zhou, 2022). However, the proven reserves of onshore tight gas in China only accounted for about 25% of the tight gas resources by the end of 2020. Therefore, accelerating the exploration and development of tight gas resources is of great significance (Jia et al., 2012, 2022). Hydraulic fracturing is one of the most important oil and gas stimulation methods, and it has been widely applied around the world in recent years (Liu. 2021). However, despite its benefits to oil and gas production, hydraulic fracturing still poses many issues regarding reservoir and environmental protection. Large-scale hydraulic fracturing requires substantial amounts of water, which presents significant challenges in arid regions (Xia and Wu, 2021). Additionally, abundant chemical additives in the water-based fracturing fluid can contaminate the shallow aquifer and surface environment (Small et al., 2014; Sakmar, 2011). Furthermore, the water-based fracturing fluid can cause clay minerals to swell, resulting in formation damage (Anderson et al., 2010). Therefore, to solve these problems, waterless fracturing is gradually proposed as an essential way to develop unconventional hydrocarbons. With the proposed carbon capture, utilization and storage (CCUS) project, CO2 is gradually being regarded as a resource for oil and gas development (Sinal and Lancaster, 1987; Wang et al., 2012). When the temperature and pressure of subsurface environment exceed 31.1 °C and 7.38 MPa, respectively, the injected CO<sub>2</sub> reaches supercritical state (Span and Wagner, 1996; Gupta et al., 2005). Supercritical CO<sub>2</sub> (SC-CO<sub>2</sub>) has many particular properties, such as water-like density and gas-like viscosity, almost zero surface tension, etc. As a result, SC-CO2 is considered a waterless fracturing fluid for exploiting unconventional hydrocarbon (Kolle, 2000; Liu et al., 2013; Yang et al., 2023). Recently, various investigations have been performed to explore the feasibility and mechanism of SC-CO<sub>2</sub> fracturing.

Initially, (Ishida et al., 2012, 2013, 2016) and Inui et al. (2014) successively carried out fracturing experiments on granite using different fluids, including viscous oil, water, liquid CO<sub>2</sub> and SC-CO<sub>2</sub>, to monitor the fracture propagation process. The results showed that low-viscosity fluids such as liquid and SC-CO<sub>2</sub> can induce more complex fractures compared to high-viscosity fluids like water and oil. Further, low-viscosity fluids mainly induce shear fractures, while high-viscosity fluids induce tensile fractures. Chen et al. (2015) and Bennour et al. (2015) conducted true-triaxial hydraulic fracturing experiments on anisotropic granite and shale samples with fluids of different viscosities, and confirmed the influence of fluid viscosity on fracture propagation mode. They discovered that relatively complex fracture networks are formed in the rock when using low-viscosity fluids like SC-CO<sub>2</sub>. Fractures induced by SC-CO<sub>2</sub> mainly propagate along mineral boundaries, while fractures generated by water and oil often penetrate through mineral particles. Wang et al. (2017) also conducted gas- and SC-CO<sub>2</sub> fracturing experiments on naturally fractured Niobrara shale samples. The results suggested that the breakdown pressure of shale fractured by SC-CO<sub>2</sub> is far below the theoretical prediction value and that of slick water fracturing, and some even fell below the minimum horizontal stress. Furthermore, Zou et al. (2018) studied the behavior of SC-CO<sub>2</sub>-induced fractures in layered tight sandstones. They concluded that the fractures induced by SC-CO2 are mainly shear failures, and most of the fracture branches induced by SC-CO<sub>2</sub> fracturing are narrower than those induced by water fracturing, which may hinder the transportation of proppants. Since SC-CO<sub>2</sub> has an extremely high leakage rate, a large pumping rate is necessary to maintain a high injection pressure, allowing the fractures to open widely and persistently.

In addition to the aforementioned research, SC-CO<sub>2</sub> fracturing experiments on artificial cement samples and transparent acrylic materials were carried out by Zhou et al. (2018a, 2018b). They discovered that the energy release rate in SC-CO<sub>2</sub> fracturing is 1–3

orders of magnitude higher than that of water fracturing. Therefore, it would lead to the formation of multi-branched fractures due to the high amount of accumulated energy that could be converted into a driving force. Also, the SC-CO<sub>2</sub> phase transition is an important cause of forming complex fractures in the fracturing process. Similarly, Zhang et al., (2019) conducted SC-CO2 fracturing experiment on shale considering the effect of anisotropy. It was found that as the bedding angle increases, the breakdown pressure of rock generally shows a downward trend. Additionally, the breakdown pressure of shale increases gradually with the increase in fluid injection rate. Recent study (Shafloot et al., 2021) on fracturing behavior of SC-CO<sub>2</sub> and water with Green River shale demonstrated that the breakdown pressure of water fracturing was two to three times greater than that of SC-CO<sub>2</sub>. Under the isotropic horizontal stress, SC-CO<sub>2</sub>-induced fracture propagation hardly depends on the bedding plane. In comparison, Yang et al. (2021a, 2021b, 2024) proposed a fracture-quantification method based on micro-CT images to investigate the fracture initiation mechanism of tight sandstone formation. The results indicated that SC-CO<sub>2</sub> fracturing tended to form more complex fracture mode, with lager roughness, fractal dimension, fracture volume fraction, etc., compared to water. Zang et al. (2023a, 2023b) conducted pre-CO<sub>2</sub> fracturing in tight sandstone using digital image correlation (DIC) method. They found that low-viscosity fluid like SC-CO<sub>2</sub> more tend to induce micro-fractures, and the fracture modes are main I-II composite fractures. The DIC method is regarded as an intuitive, accurate, and effective method for quantifying fracture characteristics. However, these rock sample used in the laboratory research is quasi-three-dimensional rock slab, and the true triaxial stress condition of the subsurface cannot be realized. Zhao et al. (2022) established a workflow that combines machine learning algorithms with the three-dimensional lattice method to investigate the fracture propagation process in four main shale fabric facies. Meanwhile, sensitivity analyses were also carried out to quantify the impacts of different control parameters on fracture propagation. Liu et al. (2023) proposed four indicators for describing wellbore deflection based on fracture morphology. Then, several fracturing designs, including stage arrangement, fracturing sequence and fracturing techniques, were applied to study the feasibility of the fan-shaped well factory design. Zhang et al. (2024) utilized the lattice method to conduct multi-scale fracture propagation in layered media and verified it through laboratory fracturing observations and field microseismic monitoring. In addition, they carried out a creep analysis of CO<sub>2</sub> fracturing in natural gas hydrates, and this research is of great significance for the long-term prediction of the geomechanical response during natural gas extraction (Tang et al., 2024).

While numerous studies have explored the fracturing process of SC-CO<sub>2</sub>, research related to the tight sandstone formation remains scarce. Current research on the fracturing of tight sandstone using supercritical CO<sub>2</sub> faces the issue of small sample sizes, typically less than 100 mm, which limits the fracture propagation area (Li et al., 2019; Yang et al., 2022). Although Zou et al. (2018) increased the sample size in their study, their quantitative analysis methods were insufficient. They performed a qualitative analysis of fracture distribution using CT imaging but did not conduct a quantitative assessment of the spatial parameters of the fractures. Therefore, it is crucial to investigate the fracture propagation characteristics of tight sandstone induced by SC-CO<sub>2</sub> fracturing, particularly with larger rock samples simulating in-situ stress conditions. This paper aims to carry out SC-CO<sub>2</sub> fracturing experiments on tight sandstone under true-triaxial conditions and reconstruct the fracture morphology. Additionally, fracture parameters such as roughness and fractal dimension will be obtained using quantitative algorithms to explore the fracture propagation characteristics. The

results are expected to provide theoretical guidance for SC-CO<sub>2</sub> fracturing craft design.

#### 2. Experimental

# 2.1. Apparatus

The SC-CO $_2$  fracturing experiment is carried out using a true-triaxial stress system (as shown in Fig. 1) that has been improved based on the SC-CO $_2$  jet equipment (Wang et al., 2018). The fracturing experimental system comprises a SC-CO $_2$  generation and injection unit, a true-triaxial stress loading unit, and a control & data monitoring unit. This system can replicate formation temperature and stress conditions and conduct fracturing experiments with a variety of fluids such as water, CO $_2$ , N $_2$ , etc.

The SC-CO<sub>2</sub> generation and injection system is composed of a  $\rm CO_2$  container, a cooling box, a high-pressure syringe pump, and a constant-temperature heating tank. The  $\rm CO_2$  container serves as the fluid source for fracturing experiments, and multiple gas cylinders are prepared to ensure an adequate supply of  $\rm CO_2$ . The cooling box is used to liquefy the gaseous  $\rm CO_2$ , which includes a refrigeration unit, a water-bath cold box, coolant, and a temperature control device. Once the  $\rm CO_2$  reaches a liquid state, it is pressurized by a high-pressure syringe pump and heated by a heating tank to exceed the critical pressure and temperature of  $\rm CO_2$  (7.38 MPa and 31.1 °C, respectively).

The true-triaxial stress loading unit is a crucial module of the fracturing experimental system and consists of a rock sample holder, a hydraulic loading unit, and an operation control unit. As shown in Fig. 2, the rock sample holder can accommodate cube rock samples with side lengths ranging from 100 to 400 mm. The heating rods situated on the side of the stress-loading cover plate are used to heat the rock sample, which can be heated up to 300 °C. The triaxial stress is independently applied along the *x*-, *y*-, and *z*-directions by the hydraulic unit and can provide a maximum triaxial stress of 60 MPa. During the experiment, the control unit enables the expected stress value and experimental temperature to be set to simulate reservoir conditions.

The control and data monitoring unit mainly control the experimental process using various sensors and data lines, and record parameters such as fluid pressure and triaxial stress in real



Fig. 2. Rock sample holder.

time. It is also used to address various abnormal conditions to ensure the progress of the experiment and the handling of safety emergencies.

#### 2.2. Sample preparation

To explore the fracture propagation characteristics of SC-CO $_2$  fracturing under reservoir conditions, tight sandstone outcrops were collected from the Chang 6 Member of Yanchang Oilfield in Shaanxi Province. The mechanical properties of the rock sample from outcrops are detailed in Table 1. To facilitate better observation of fracture morphology and considering the original size of the outcrop, a standard sample with a side length of 300 mm was selected as the experimental specimen. Subsequently, a simulated borehole, perpendicular to the bedding plane, was drilled with a depth of 160 mm and a diameter of 16 mm. A steel pipe, with an outer diameter of 14 mm and a length of 140 mm, was affixed to the borehole to serve as a channel for fluid injection. As illustrated in Fig. 3, a 20 mm open-hole section at bottom of the borehole was

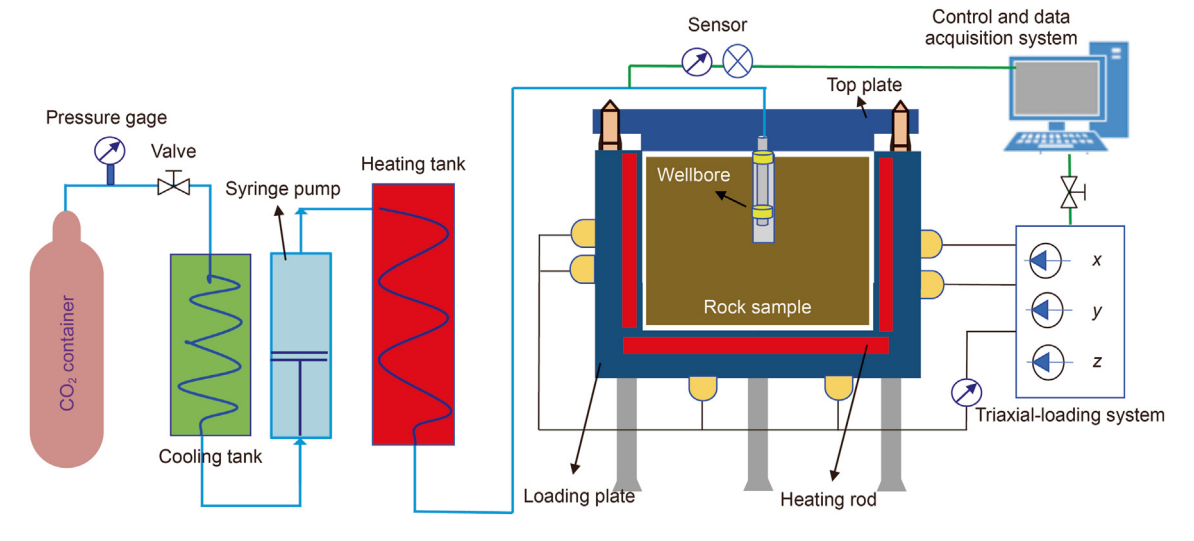


Fig. 1. Diagram of the true-triaxial fracturing system.

Table 1
Mechanical properties of tight sandstone collected from Chang 6 Member.

Density, g/cm <sup>3</sup>	Compressive strength, MPa	Tensile strength, MPa	Elastic modulus, GPa	Poisson's ratio	Permeability, $10^{-12} \text{ m}^2$	Porosity, %
2.67	186.5	5.3	13.826	0.276	0.01115	4.89

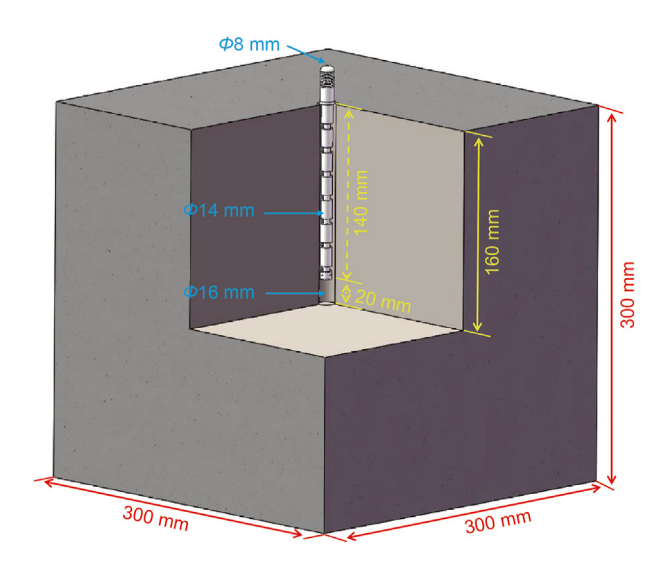


Fig. 3. Diagram of standard rock sample.

intentionally left after cementing.

# 2.3. Experimental procedure

To investigate the fracture propagation behavior, fracturing experiments were conducted using water and SC-CO<sub>2</sub> under various in-situ stress conditions. Based on the geological data from the tight reservoir of Chang 6 Member in Yanchang Oilfield, the maximum horizontal principal stress is distributed within the range of 40–47 MPa, the minimum horizontal principal stress falls within 34–38 MPa, and the difference in the horizontal principal stress is distributed in the range of 2–9 MPa. Therefore, to simulate the geological stress conditions, a similar horizontal stress difference was applied in the experimental process. The experimental scheme is outlined in Table 2.

This paper presents a detailed description of the experimental procedures employed to investigate the fracture characteristics of rock samples subjected to SC-CO<sub>2</sub> injection. The experimental protocol consists of the following key steps: (1) Experimental preparation. This stage involves preparing CO<sub>2</sub> source, ensuring the pipeline's tightness, and vacuuming the pipeline to remove any impurities and air. Additionally, the tight sandstone sample is heated

to the desired testing temperature according to the experimental plan. (2) Rock sample installation and stress loading. The prepared rock sample is placed into the triaixal holder, then the heating unit of triaxial loading system is activated to maintain the required temperature. Triaxial stress is then applied to the rock sample, beginning with the application of the minimum horizontal principal stress to a specified value, followed by applying the maximum principal stress at the same loading rate. The principal stresses in two horizontal directions are brought to the target pressure through alternate loading. Finally, the vertical stress is applied. (3) SC-CO<sub>2</sub> generation and injection. CO2 is released from a steel cylinder and passed through a cooling unit to convert it into a liquid state. The liquid CO<sub>2</sub> is then pumped into a heating tank to elevate its temperature to the supercritical state, which is the desired phase for injection into the wellbore. (4) Data monitoring and experimental control. Throughout the injection of fracturing fluid, the entire experiment is monitored and controlled by a control system, various parameters such as temperature, pressure, and other relevant data are continuously monitored in real-time. (5) Dye fluid injection. After rock is fractured, unload the triaxial stress is applied to the rock samples. Dye fluid is injected into the fractured rock sample with a low injection rate, pressure variations and fluid flow trajectories of dye fluid are recorded to capture the fracture propagation characteristics. (6) Fracture surface scanning. The fracture surfaces are eventually scanned using a contactless micromorphological scanner, a series of algorithms are then employed to analyze the quantitative properties of fracture surfaces.

# 2.4. Quantitative algorithm for fracture morphology

This section delves into the examination of the topographical attributes of fractures induced by SC-CO<sub>2</sub> through a contactless micromorphological scanner. The stereo images depicting the fracture surface are presented in Fig. 4. To acquire quantitative insight into these fractures, we derive the areal roughness and complexity parameters from height images utilizing a series of algorithms. The roughness of fracture surface is quantified by the maximum height of surface ( $S_z$ ), and the root mean square (RMS) ( $S_q$ ) of the height distribution. The  $S_z$  is defined as height difference between the highest peak and the deepest valley within the specified sampling area. The RMS ( $S_q$ ) is characterized as standard deviation of the height distribution (Jia et al., 2018), and can be calculated using the following formula:

**Table 2** Experimental schemes of fracturing with water and SC-CO<sub>2</sub>.

Number	Fluid	Temperature <i>T</i> , °C	Injection rate Q, mL/min	$\sigma_{\rm V}/\sigma_{\rm H}/\sigma_{\rm h}$ , MPa
Y0	Water	40	20	16/12/8
Y1, Y2	SC-CO <sub>2</sub>	40	40	16/12/12
Y3, Y4				16/12/10
Y5, Y6				16/12/8
Y7, Y8				16/12/6
Y9, Y10				16/12/4
Y11				16/18/12
Y12				16/18/16

Note:  $\sigma_V$ -vertical principal stress;  $\sigma_H$ -maximum horizontal principal stress;  $\sigma_h$ -minimum horizontal principal stress.

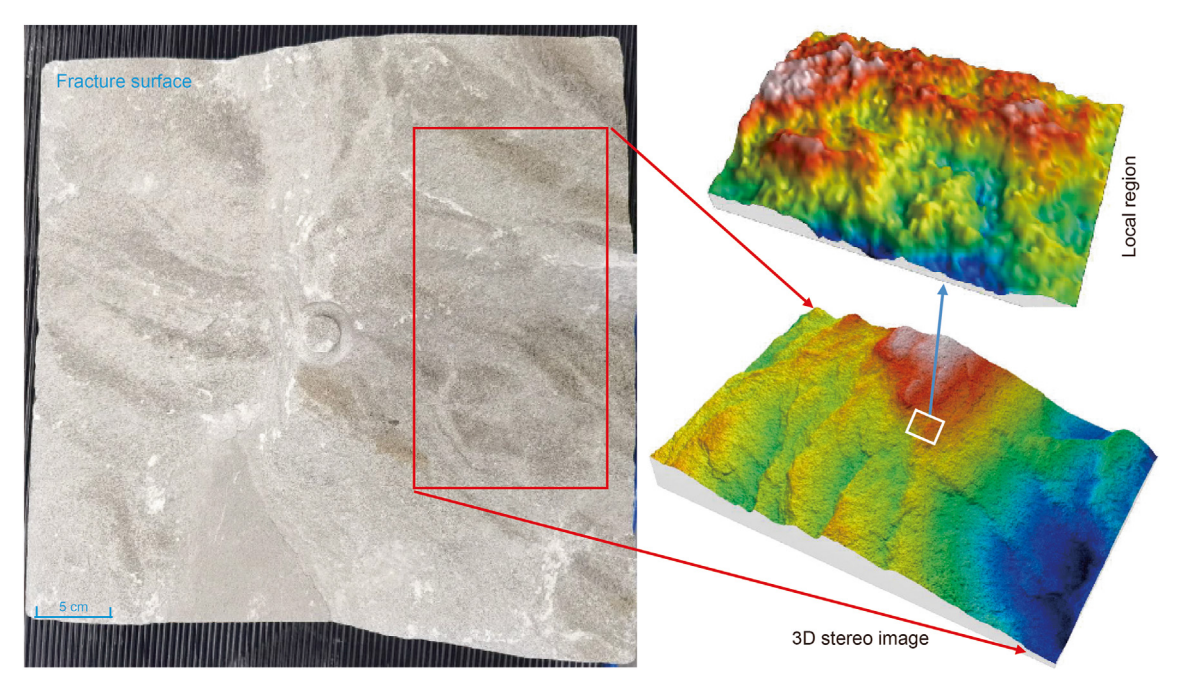


Fig. 4. Micromorphological scanning image analysis of fracture surface.

$$S_{\mathbf{q}} = \sqrt{\frac{1}{A} \int_{A} z^{2}(x, y) \mathrm{d}x \mathrm{d}y} \tag{1}$$

where A represents the sampling area of fracture surface; z(x, y) denotes the maximum height in different position.

The complexity of fracture morphology is delineated through the parameter of fractal dimension (*FD*). It is a statistical index of complexity comparing how detail in a fractal pattern change with the scale at which it is measured (Yang et al., 2021a). In this study, a box-counting method is employed to calculate fractal dimension (*FD*), which is expressed as follows (Bonnet et al., 2001; Falconer, 2014):

$$FD = \lim_{r \to 0} \frac{\ln(N_r)}{\ln(1/r)} \tag{2}$$

where  $N_{\rm r}$  corresponds to the number of boxes with size r needed to cover the structure. For a 3D fracture surface, 2 < FD < 3 and a larger FD value means a relatively complex surface, while a smaller FD describes a surface with less complexity (Dutilleul et al., 2015).

Furthermore, tortuosity  $(T_0)$  serves as another crucial parameter for characterizing fracture morphology. It is defined as the ratio of the total length  $(L_f)$  to the linear length  $(L_0)$  between the two ends of fracture, which can be obtained using the methodology illustrated in Fig. 5 and Eq. (3) (Li et al., 2019).

$$T_0 = \frac{L_f}{L_0} \tag{3}$$

# 3. Experimental results of water and SC-CO<sub>2</sub> fracturing

In this section, the fluid pressure curves for both water and SC-CO<sub>2</sub> fracturing are recorded, and breakdown pressures (BP) under various in-situ stress conditions are discussed. Subsequently, the spatial morphologies of induced fractures are reconstructed for a

comprehensive understanding of the fracturing process. The quantitative characteristics of fracture surface are investigated using advanced algorithms, providing insights into the intricate details of the fractures. Furthermore, the fracture propagation characteristics of SC-CO<sub>2</sub> fracturing in tight reservoirs are analyzed.

# 3.1. The curve of fluid pressure during water and SC-CO<sub>2</sub> fracturing

The fluid pressure responses during water and SC-CO<sub>2</sub> fracturing, conducted under identical stress conditions, are depicted and compared in Fig. 6. During the initial stage of water fracturing, the fluid pressure exhibited a gradual increase characterized by a modest growth rate. Subsequently, it transitioned to a second stage within a very brief timeframe, marked by a pronounced and accelerated increase in pressure. Upon reaching a fluid pressure of 17.1 MPa, a transient pressure drop ensued, signaling the initiation of localized fractures within the rock mass. Following this pressure fluctuation, there was a subsequent rise in fluid pressure, manifesting two distinct effects: firstly, the expansion of pre-existing fractures, and secondly, continued pressurization of the fluid in the unfractured region, leading to the initiation of additional fractures. This dynamic pressure behavior indicates that the largersized rock sample offers a relatively ample space conducive to effective fracture propagation under true-triaxial conditions.

Unlike water fracturing, the pressure evolution during SC-CO<sub>2</sub> fracturing can be delineated into three distinct stages: In the initial phase of fluid injection, the pump pressure undergoes a linear and gradual increase until surpassing the critical pressure of  $CO_2$ , constituting approximately half of the entire experimental process (around 15 min). This prolonged duration is attributed to the pronounced compressibility of  $CO_2$ , necessitating considerable time for fluid compression. Consequently, the pressure experiences a relatively low growth rate before reaching the critical value. Upon fluid injection, there is a swift escalation in pressure until the rock undergoes breakdown, represented by the peak of the pressure curve. This stage exhibits a higher-pressure growth rate compared to the initial phase, and the time required is only about a quarter of the initial period. This phenomenon signifies that  $CO_2$  has attained its

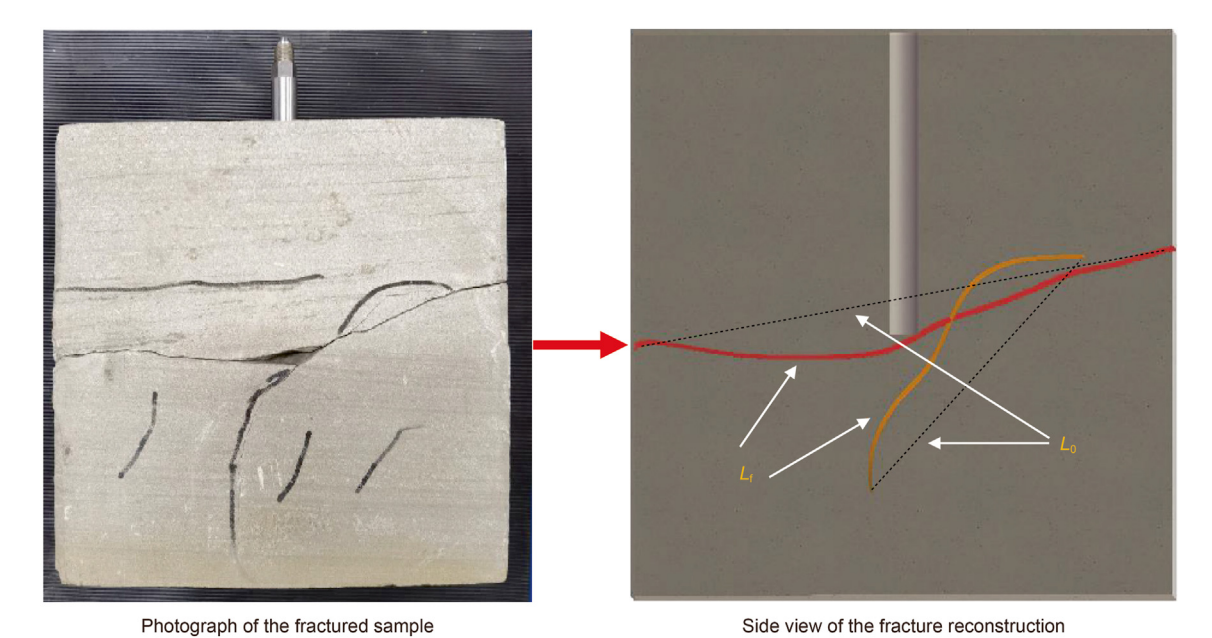


Fig. 5. The schematic of tortuosity calculation method for fractured rock sample.

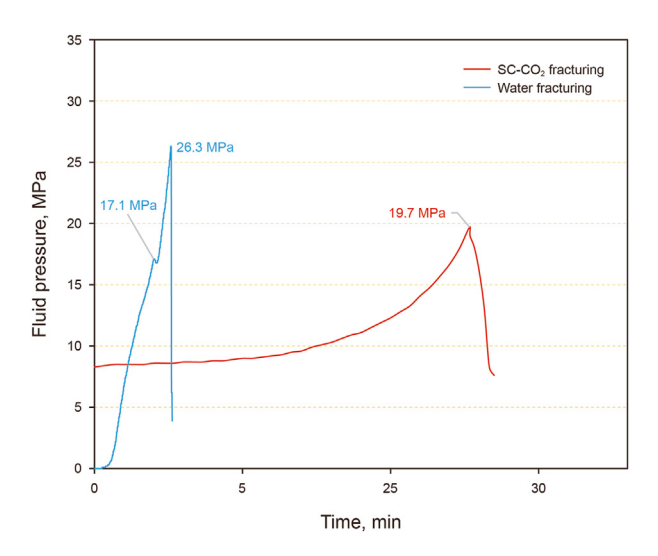


Fig. 6. Fluid pressure profiles in water and SC-CO<sub>2</sub> fracturing.

compression limit during this stage, leading to a rapid elevation in fluid pressure through continuous compression of fluid volume. Following rock breakdown, SC-CO<sub>2</sub> is released from the fracture to the outlet of the sample holder. The pressure curve undergoes an instantaneously drop, accompanied by the observation of white smoky solid—liquid miscible CO<sub>2</sub> at the outlet. The phenomenon is attributed to the dynamics of fluid volume expansion during the instantaneous release process, leading to a significant temperature drop.

This temperature decrease triggers the phase transition of SC-CO<sub>2</sub> due to the Joule—Thomson effect. As the fluid volume is compressed, SC-CO<sub>2</sub> would accumulate and pressurize in the wellbore, penetrating into the inner rock formations (Zhou et al., 2019). The critical turning point in this process occurs when the BP of the rock is reached. At this juncture, high-energy CO<sub>2</sub> is released instantaneously. This sudden release induces the rapid propagation of

fractures throughout the rock, extending to the rock boundary, accompanied by a sharp decline in fluid pressure. This distinctive process sets SC-CO<sub>2</sub> fracturing apart from water fracturing. It serves as additional confirmation that SC-CO<sub>2</sub> has the capability to reduce the BP of rocks. The magnitude of this reduction is quantified at approximately 25.1%, as detailed in Table 3. This reduction in BP further highlights the efficacy of SC-CO<sub>2</sub> as a fracturing fluid with potential advantages over traditional water-based methods.

# 3.2. The effect of in-situ stress on breakdown pressure

In accordance with the fluid pressure curve, the BP of rocks subjected to SC-CO<sub>2</sub> induced fractures under varying in-situ stresses has been determined and is presented in both Table 3 and Fig. 7. The key observation is that, while keeping the vertical stress and the maximum horizontal principal stress constant, an increase in the horizontal principal stress difference (HPSD) results in a gradual decrease in the BP of the rock. Specifically, at an HPSD of 8 MPa, the rock exhibits heightened susceptibility to fracturing, attaining an average BP of 15.1 MPa. Conversely, at an HPSD of 0 MPa, the average BP of rock samples fractured by SC-CO<sub>2</sub> is recorded at 23.6 MPa. The significant reduction in BP becomes evident when the HPSD increases from 0 to 8 MPa, resulting in a nearly 36% decrease in the BP of the rock. This result aligns with classical fracture mechanics principles (Hubbert and Willis, 1957).

The fractures induced by SC-CO<sub>2</sub> in rock samples Y11 and Y12 were investigated under abnormal in-situ stress conditions. The findings demonstrate that elevating the maximum horizontal principal stress to 18 MPa, based on the Y1 rock sample, results in a notable 76% increase in the BP of the rock. Furthermore, proceeding from rock sample Y11, an additional increase in the minimum horizontal principal stress to 16 MPa (Y12) is implemented, aligning it with the vertical stress magnitude. It is discerned that the BP of the rock continues to escalate, registering a 6.3% increment over that of the Y11 rock specimen. This empirical evidence underscores the pronounced influence of in-situ stress conditions on the BP of the rock.

**Table 3**Breakdown pressure (BP) under different in-situ stresses.

Number	Fluid	Temperature T, °C	Flow rate Q, mL/min	$\sigma_{\rm V}/\sigma_{\rm H}/\sigma_{\rm h}$ , MPa	Average BP, MPa
Y0	Water	40	20	16/12/8	26.3
Y1, Y2	SC-CO <sub>2</sub>	40	40	16/12/12	23.6
Y3, Y4				16/12/10	22.0
Y5, Y6				16/12/8	19.7
Y7, Y8				16/12/6	17.5
Y9, Y10				16/12/4	15.1
Y11				16/18/12	25.4
Y12				16/18/16	27.0

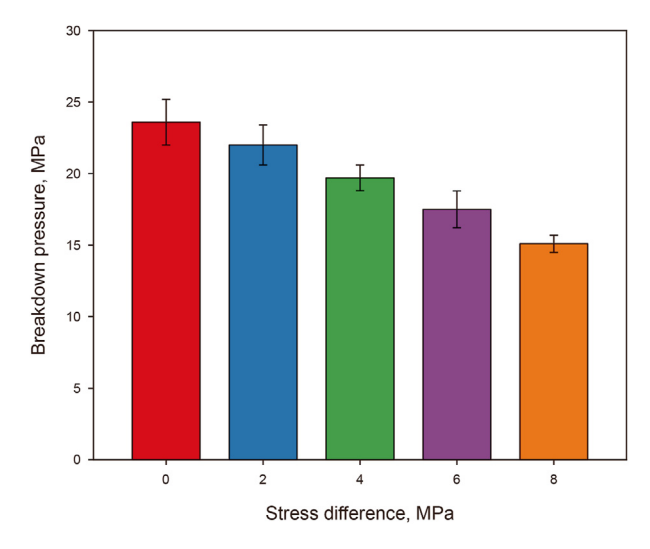


Fig. 7. The change of breakdown pressure of rock with HPSD.

# 3.3. Fracture geometry induced by SC-CO<sub>2</sub> under different in-situ stresses

After a rock is fractured, dyed tracer fluid was injected into the fractured rock at a low injection rate, and the trajectory of the tracer fluid flow was meticulously recorded as the fracture propagation



Fig. 8. Fracture obtained through dye fluid injection.

path, as depicted in Fig. 8. The spatial morphology of the induced fracture under varying in-situ stress conditions was reconstructed based on the delineated dye-marked areas. The original fractured sample and the three-dimensional (3D) reconstruction results of the same size are visually presented in Figs. 9–16. Fig. 9 indicates that water-induced fractures tend to propagate predominantly along the horizontal bedding direction, with a notable fracture branch emerging at the boundary of the minimum horizontal principal stress direction. However, this observation appears to deviate from the predictions of classical fracture mechanics theory, where fractures are expected to propagate orthogonally to the minimum principal stress direction. The apparent inconsistency is hypothesized to be rooted in the composition of the original rock bedding, which contains clay minerals. The introduction of water induces clay swelling, consequently diminishing the strength of the rock. Another contributing factor could be the weak cementation present in the initial bedding plane. Consequently, it renders the fractures more prone to initiation and propagation along the inherently feeble surfaces of the bedding.

Under identical experimental conditions, the fracture morphology induced by SC-CO<sub>2</sub> is illustrated in Fig. 12. It is discernible that primary fractures initiate proximate to the wellbore and subsequently propagate approximately along the diagonal direction, accompanied by the presence of numerous microfractures around the wellbore vicinity. Moreover, two secondary fractures intersecting with the principal fracture are observed. The spatial distribution characteristics of these fractures align with the overarching principles of classical fracture mechanics theory.

Figs. 10–14 illustrate the spatial morphology of fractures induced by SC-CO2 under various stress differentials. Analysis of Fig. 10 reveals that, in conditions where the maximum and minimum horizontal principal stresses are equivalent (HPSD is 0), SC-CO<sub>2</sub> initiates complex fracture networks within the rock matrix. Predominantly, a curved primary fracture, oriented approximately perpendicular to the wellbore, emerges in proximity to the wellbore and extends laterally through the entire rock sample. Additionally, a secondary fracture, roughly parallel to the horizontal bedding plane, develops in the upper segment of the primary fracture; however, this secondary fracture only propagates halfway through the rock sample. Further, numerous branching fractures, intersecting the direction of the maximum horizontal principal stress, manifest adjacent to the main fracture. These observations indicate that under an HPSD of 0, fracture propagation is influenced not only by the bedding plane, which leads to the formation of horizontal fractures nearly vertical to the wellbore; but also by the in-situ stress, leading to the development of secondary fractures that are approximately perpendicular to a specific horizontal principal stress direction. Overall, the fracture morphologies exhibit diversity and complexity under this stress scenario. Contrastingly, when the HPSD is elevated to 2 MPa (as shown in Fig. 11), distinct fracture propagation patterns are observed, albeit with fewer fractures compared to the Y1 rock sample. As the HPSD

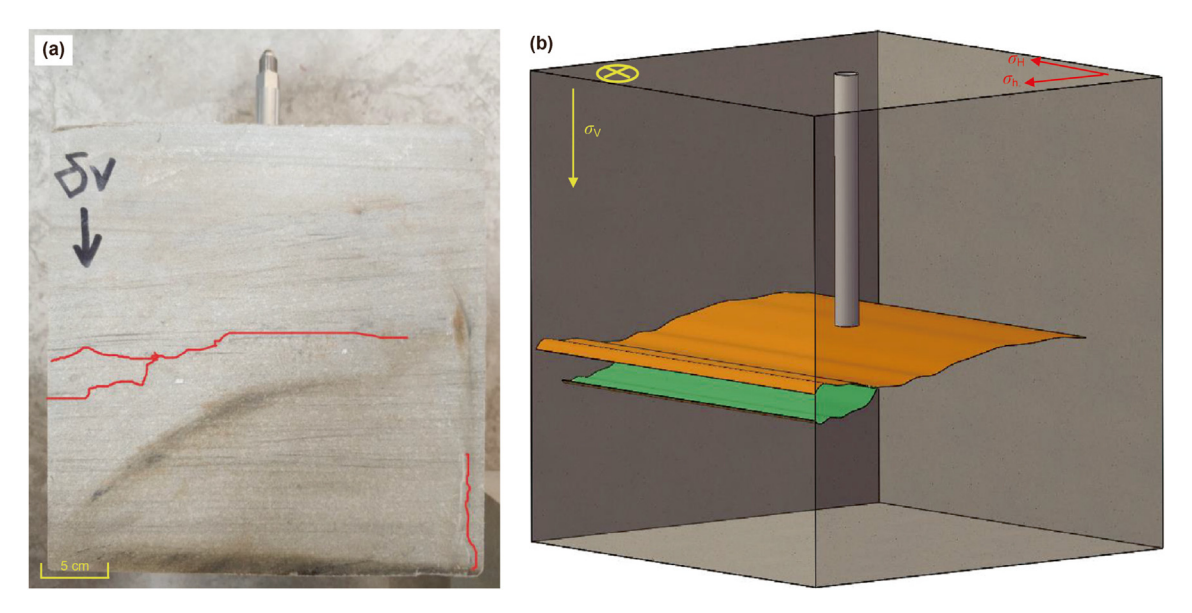


Fig. 9. The picture of fractured rock and the fracture reconstruction profile induced by water (Y0:  $\sigma_V/\sigma_H/\sigma_h$  of 16/12/8 MPa).

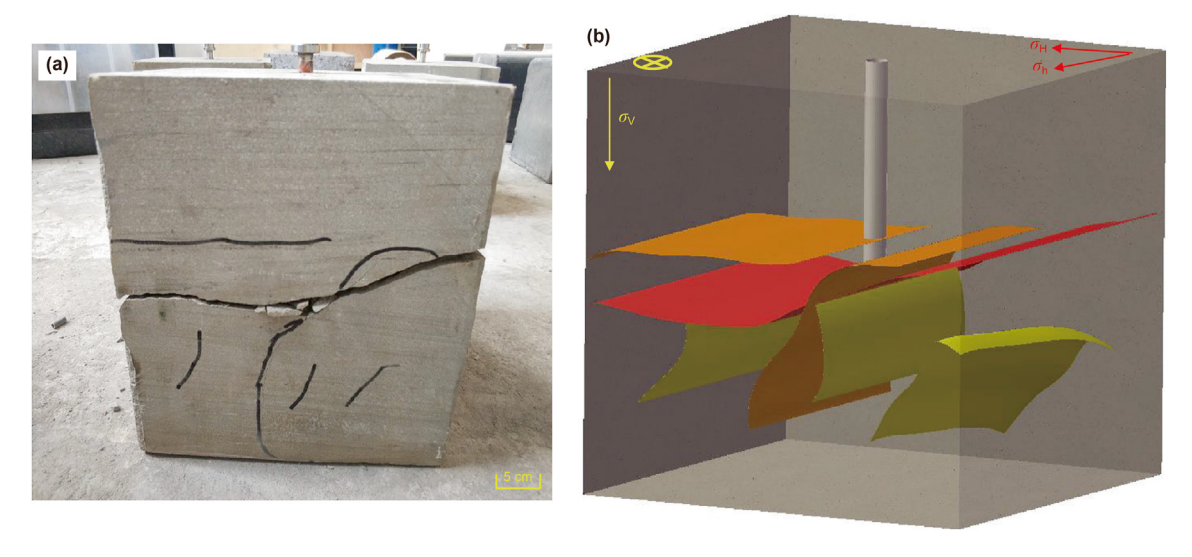


Fig. 10. The picture of fractured rock and the fracture reconstruction profile induced by SC-CO<sub>2</sub> under  $\sigma_V/\sigma_H/\sigma_h$  of 16/12/12 MPa (Y1).

increases further, there is a gradual decline in the number of induced fractures, and the spatial configuration of the fractures simplifies.

Moreover, as depicted in Figs. 13 and 14, with continued escalation of the HPSD, SC-CO<sub>2</sub> tends to induce a main fracture propagating along the diagonal axis, accompanied by a limited amount of secondary fractures generated on one side of the primary fracture. Summarily, an increase in the HPSD applied to the rock contributes to a reduction in the BP of the rock. However, this escalation in HPSD is associated with a tendency to generate a singular fracture pattern, highlighting a pronounced influence of in-situ stress differences on fracture propagation. Conversely, as the HPSD decreases, SC-CO<sub>2</sub> tends to induce complex fracture networks, characterized by more diverse propagation directions. This suggests that the fracture propagation process is affected by a combination of rock properties and in-situ stress conditions.

Additionally, abnormal stress significantly impacts fracture morphology. Figs. 15 and 16 illustrate the fracture propagation

patterns under conditions where the maximum horizontal principal stress exceeds the vertical stress. In Fig. 15, with the maximum horizontal principal stress acting as the predominant stress on the rock, the difference between the vertical stress and the minimum horizontal principal stress is 4 MPa. Under these conditions, SC-CO<sub>2</sub> induces two intersecting fractures near the wellbore. The fractures' wings are symmetrically distributed, intersecting or perpendicular to the wellbore. The fracture intersecting the wellbore (depicted in yellow) aligns closely with classical fracture mechanics theory. However, the presence of another fracture distribution, approximately perpendicular to the wellbore, indicates the vital influence of bedding planes on fracture propagation. When the minimum horizontal principal stress is increased to equate the vertical stress, as illustrated in Fig. 16, the spatial distribution of fractures is revealed. Numerous approximately parallel fractures intersect the wellbore, predominantly propagating obliquely. This observation underscores the collaborative impact of original bedding planes and applied stress conditions on fracture propagation. Importantly,

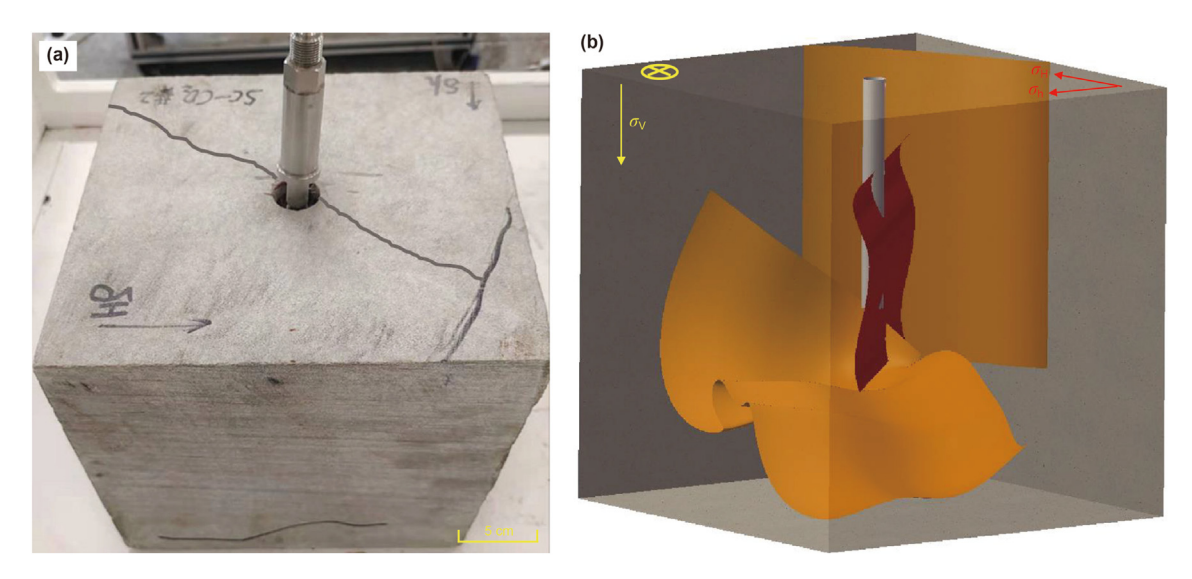


Fig. 11. The picture of fractured rock and the fracture reconstruction profile induced by SC-CO<sub>2</sub> under  $\sigma_V/\sigma_H/\sigma_h$  of 16/12/10 MPa (Y3).

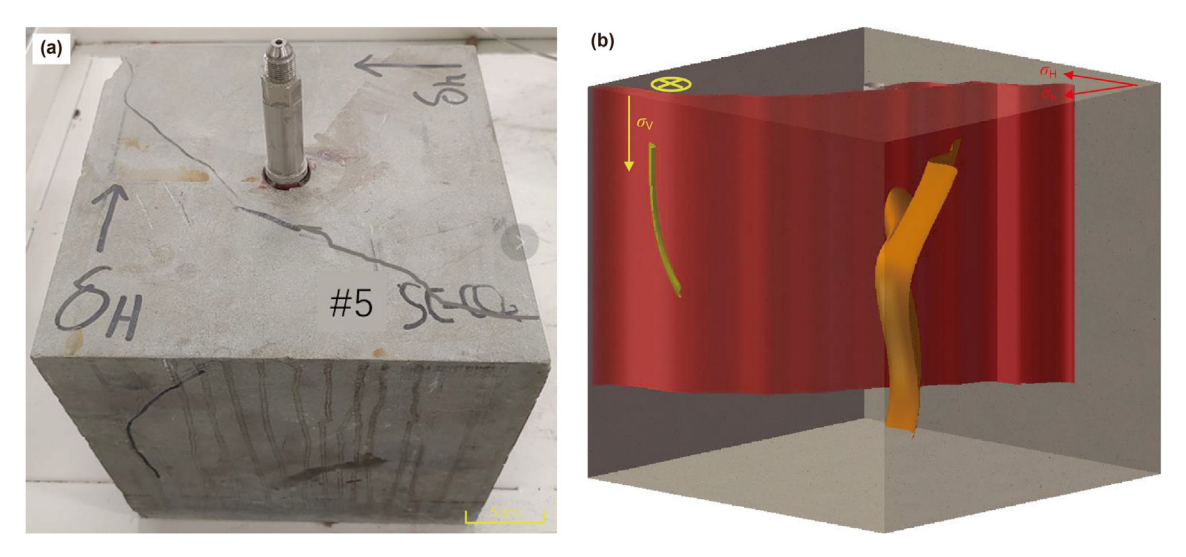


Fig. 12. The picture of fractured rock and the fracture reconstruction profile induced by SC-CO<sub>2</sub> under  $\sigma_V/\sigma_H/\sigma_h$  of 16/12/8 MPa (Y5).

this outcome parallels findings from sample Y1, substantiating that smaller stress differences contribute to the induction of more intricate fracture patterns.

# 3.4. Quantitative topography characteristics of fracture induced by $SC-CO_2$

# 3.4.1. Quantitative properties of fractures induced by water and SC- $CO_2$

Fig. 17 displays the three-dimensional (3D) morphology of local fracture surface produced by water and SC-CO<sub>2</sub> fracturing. Leveraging the 3D fracture surface morphology and employing a set of quantitative calculation methods, parameters such as  $S_q$ , FD and  $T_0$  are subsequently obtained. As depicted in Fig. 18, it can be found that, under identical stress conditions, the average maximum height ( $S_z$ ) and RMS ( $S_q$ ) of the fracture surface induced by SC-CO<sub>2</sub> fracturing are higher than those of water fracturing. Specifically, the  $S_q$  for the fracture surface induced by SC-CO<sub>2</sub> (220.5  $\mu$ m) is 2.49 times greater than that of water fracturing (88.58  $\mu$ m), indicating a higher degree of roughness in the fracture surface induced by SC-

CO<sub>2</sub>. Additionally, Fig. 19 shows the *FD* of fractures induced by the two different fluids. The *FD* of the fracture induced by SC-CO<sub>2</sub> fracturing (2.2825) is observed to be 6.5% higher than that induced by water fracturing (2.144). This finding manifests the heightened complexity of fractures induced by SC-CO<sub>2</sub> compared to those induced by water, as indicated by the higher *FD* value. These quantitative results contribute to a comprehensive understanding of the distinct morphological characteristics and complexities associated with fractures induced by water and SC-CO<sub>2</sub> fracturing processes.

Furthermore, the tortuosity ( $T_0$ ) of fractures induced by water and SC-CO<sub>2</sub> fracturing, as shown in Fig. 20, is examined from different view perspectives. Notably, the  $T_0$  of fractures induced by SC-CO<sub>2</sub> fracturing (ranging from 1.042 to 1.223) is higher than that of water fracturing (ranging from 1.018 to 1.032). Specifically, the  $T_0$  obtained from the side view are on average 2.6% higher for SC-CO<sub>2</sub>-induced fractures compared to water-induced fractures. This observation implies that SC-CO<sub>2</sub> has a tendency to induce curved fractures. The spatial distribution of fractures induced by SC-CO<sub>2</sub> is noted to be more complex, and this complexity is deemed

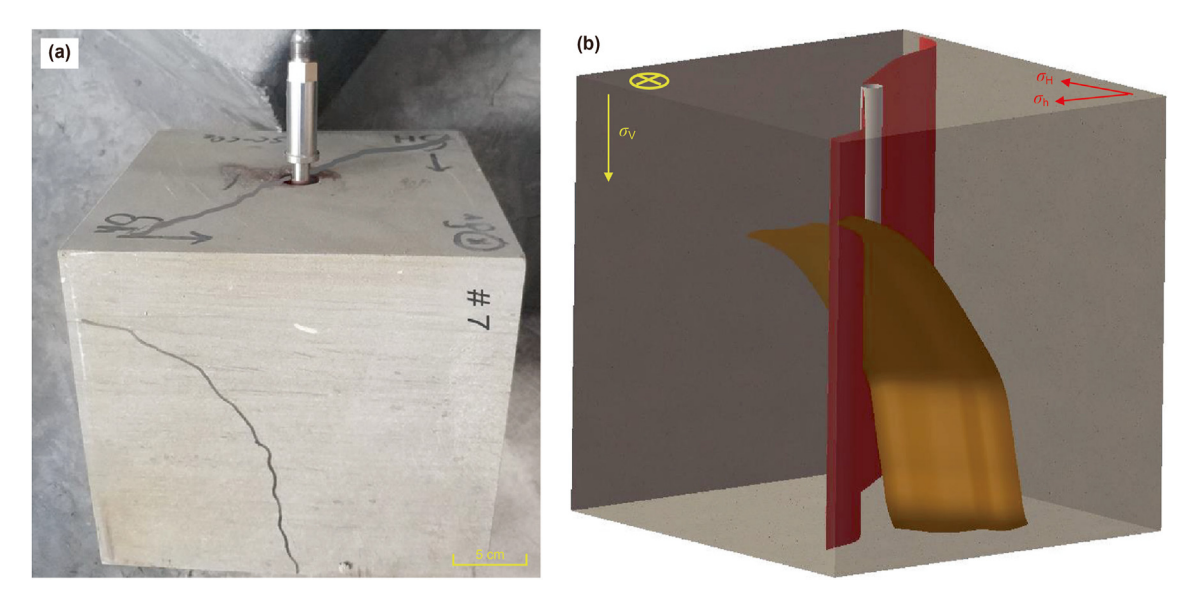


Fig. 13. The picture of fractured rock and the fracture reconstruction profile induced by SC-CO<sub>2</sub> under  $\sigma_V/\sigma_H/\sigma_h$  of 16/12/6 MPa (Y7).

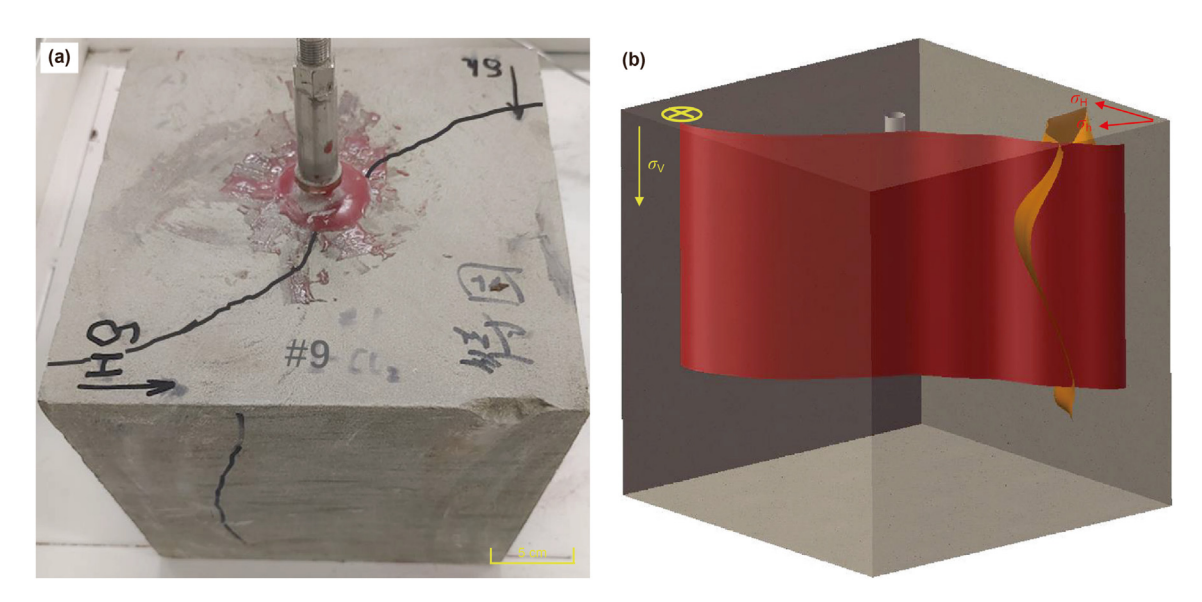


Fig. 14. The picture of fractured rock and the fracture reconstruction profile induced by SC-CO<sub>2</sub> under  $\sigma_V/\sigma_H/\sigma_h$  of 16/12/4 MPa (Y9).

advantageous for facilitating communication with the original pore channels of the formation.

The presented results indicate that SC-CO<sub>2</sub> fracturing can engender complex fracture patterns characterized by a rougher surface and a more heterogeneous spatial distribution. This result can be attributed primarily to the distinctive properties of fluid viscosity, permeability, and compressibility. In contrast to conventional water-based fracturing fluids, SC-CO2 exhibits notably low viscosity coupled with robust permeability. This unique fluid behavior facilitates its penetration into minuscule rock pores, consequently inducing localized increases in pore pressure throughout the fracturing process. This localized pressurization leads to a reduction in the BP of the rock and, consequently, a heightened incidence of micro-fractures (Yang et al., 2021b). Additionally, the pronounced compressibility of SC-CO<sub>2</sub> extends the duration of the fracturing process, allowing the fluid to more thoroughly permeate the formation and facilitate local pressurization. This extended and comprehensive fluid interaction

contributes to the induction of more tortuous and complex fracture morphologies.

3.4.2. The impact of in-situ stress conditions on the quantitative characteristics of fracture

Fractures induced by SC-CO<sub>2</sub> fracturing under diverse in-situ stress conditions were systematically examined and analyzed. Employing the quantitative characterization method for fractures (Eqs. (1)–(3)), essential parameters including the maximum height ( $S_2$ ), RMS of fracture height ( $S_q$ ), fractal dimension (FD) and the tortuosity ( $T_0$ ) were derived, with the results presented in Figs. (21)–(23).

It is evident from the findings that all four quantitative parameters exhibit a consistent decrease with the increment of HPSD, as illustrated in Fig. 21. Specifically, as HPSD increases from 0 to 8 MPa, both  $S_z$  and  $S_q$  register reductions of approximately 66.7% and 65.0%, respectively. This phenomenon indicates a diminishing roughness of the fracture surface in response to the augmentation

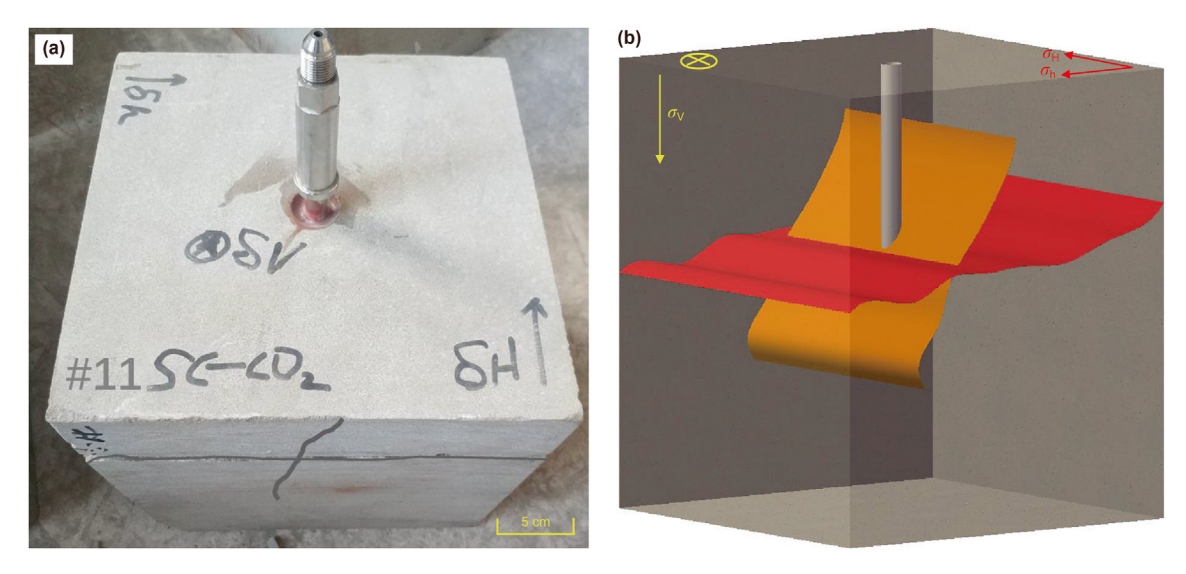


**Fig. 15.** The fracture reconstruction profile induced by SC-CO<sub>2</sub> under  $\sigma_V/\sigma_H/\sigma_h$  of 16/18/12 MPa (Y11).

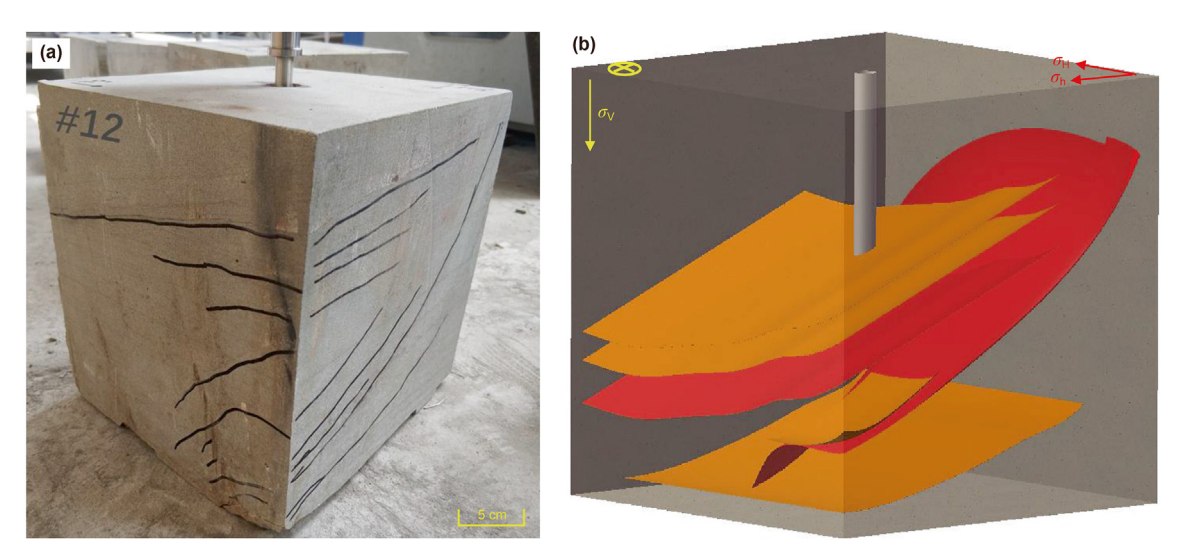


**Fig. 16.** The fracture reconstruction profile induced by SC-CO<sub>2</sub> under  $\sigma_V/\sigma_H/\sigma_h$  of 16/18/16 MPa (Y12).

of stress difference. Furthermore, the FD of fractures exhibits a declining trend with the increase in HPSD, as demonstrated in Fig. 22. When the stress difference varies from 0 to 8 MPa, the FD declines by nearly 6.2%, indicating that higher stress difference can induce a simpler fractures pattern. This deduction is further substantiated by the analysis of fracture tortuosity results (refer to Fig. 23). The findings reveal that with the improvement of HPSD, the mean value of  $T_0$  obtained from various perspectives tends to decrease. Specifically, when HPSD is 0, the mean tortuosity is 1.121, and with an increase in HPSD to 8 MPa, the average tortuosity decreases by about 7%. These results collectively indicate that higher stress differentials tend to produce flatter fractures.

When the maximum horizontal principal stress is held constant, a greater stress difference implies a lesser minimum horizontal principal stress, resulting in lower constrained strength applied to the rock sample. As concluded in Section 3.1, under these conditions, rock samples exhibit a smaller BP, making the induced fractures more prone to propagate perpendicular to the minimum principal stress direction. Consequently, the spatial distribution of fractures is relative simple, and the magnitude of tortuosity and

complexity is lower. Conversely, when the stress difference decreases, indicating that the minimum horizontal stress is closer to the maximum stress, the rock experiences a higher degree of external stress loads during fracturing. As a result, the SC-CO<sub>2</sub> fluid needs to overcome more energy to induce rock breakdown, leading to an increase in rock BP. Additionally, with the instantaneous release of high-energy CO<sub>2</sub> fluid, the induced fractures propagate in diversified directions, causing the spatial distribution of fractures to become more random and complex. Consequently, the roughness and tortuosity of fracture surfaces increase as well.

#### 4. Discussion

# 4.1. The comparison between water and SC-CO<sub>2</sub> fracturing

During water fracturing, significant fluctuations in pressure curve are observed, indicating the existence of localized fracture initiation upon fluid injection into rock. Subsequently, the fluid pressure continues to rise until reaching the BP of the rock sample, causing the entire sample to be fractured. This dynamic pressure

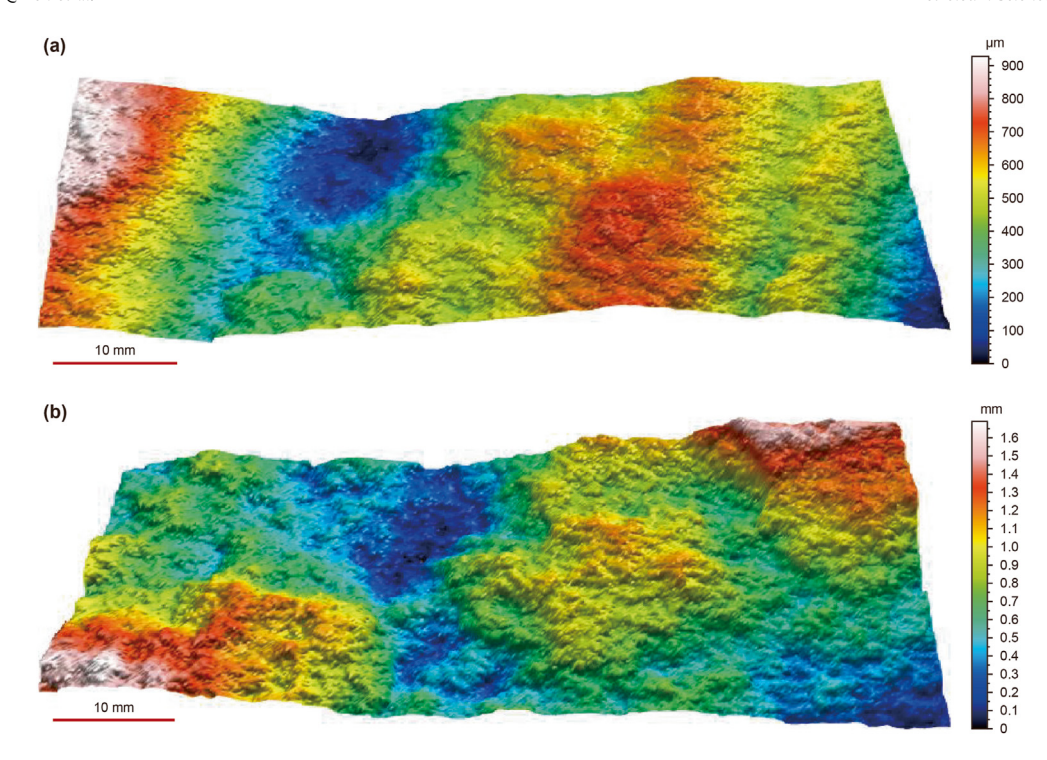
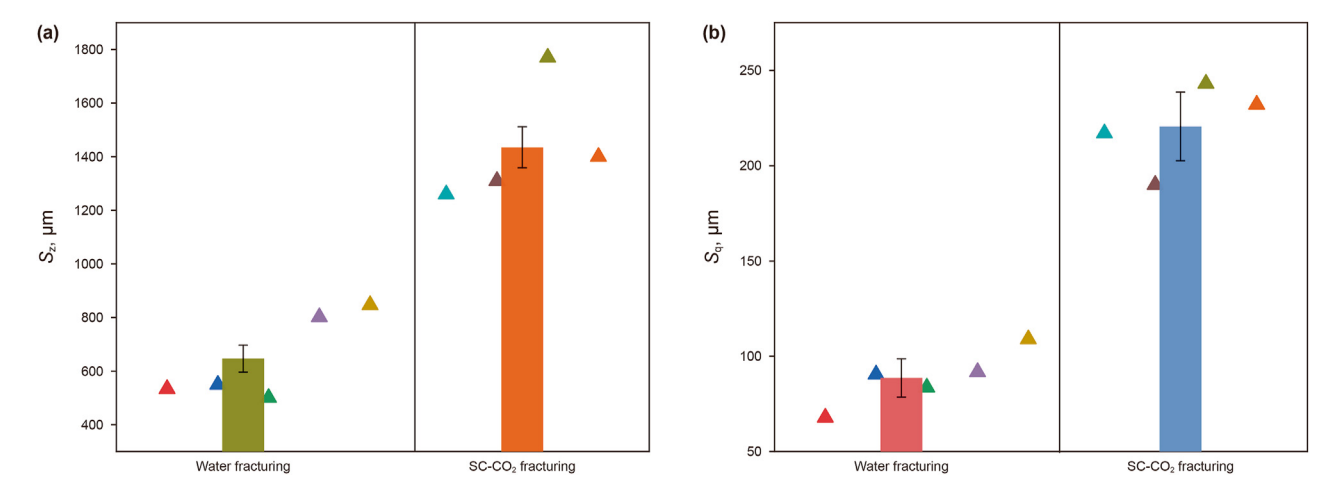


Fig. 17. The fracture surface morphology induced by water (a) and SC-CO<sub>2</sub> (b).



**Fig. 18.** The  $S_z(\mathbf{a})$  and  $S_q(\mathbf{b})$  of fracture surface induced by water and SC-CO<sub>2</sub> (the triangle represents  $S_z$  or  $S_q$  value of a single fracture, and the bar represents the mean value of  $S_z$  or  $S_q$ ).

behavior indicates that the larger-sized rock sample offers a relatively ample space conducive to effective fracture propagation under true-triaxial conditions. The heterogeneity or microstructural differences within the rock significantly influence the fracturing results. Conversely, such phenomena are absent in small-scale rock samples (Li et al., 2019). These findings contribute to a nuanced understanding of the complex interplay between fluid pressures and fracture initiation in the context of hydraulic fracturing in geological formations.

The SC-CO<sub>2</sub> fracturing curve illustrates that it consumes a significant amount of time for fluid compression. However, once the fluid reaches its compression limit, the pressure rapidly increases until the rock fractures completely. This prolonged fluid compression facilitates CO<sub>2</sub> penetration into small pore spaces, thereby reducing the local pressure differential. This process promotes rock

fracturing and decreases the BP of the rock. The magnitude of this reduction is quantified at approximately 25.1%. The pressure curve during this fracturing process is similar to the results obtained by Zou et al. (2018) and Li et al. (2019); however, there are differences in the time consumed, which is determined by the injection rate of fluid and the properties of the rock. Overall, SC-CO<sub>2</sub> can reduce the BP of the rock compared to high-viscosity fracturing fluids. On the other hand, upon instantaneous rock fracturing, a substantial amount of compression energy of fluid releases, which induces the formation of more numerous and complex fractures in the rock.

Conventional fracture mechanics and continuum mechanics typically expresses fracture initiation as a function of the stress loading and tensile strength of the rock. Under triaxial condition, the plane of fracture or parting is first tended to be perpendicular to the least principal stress. The formation BP ( $P_b$ ) can be expressed as

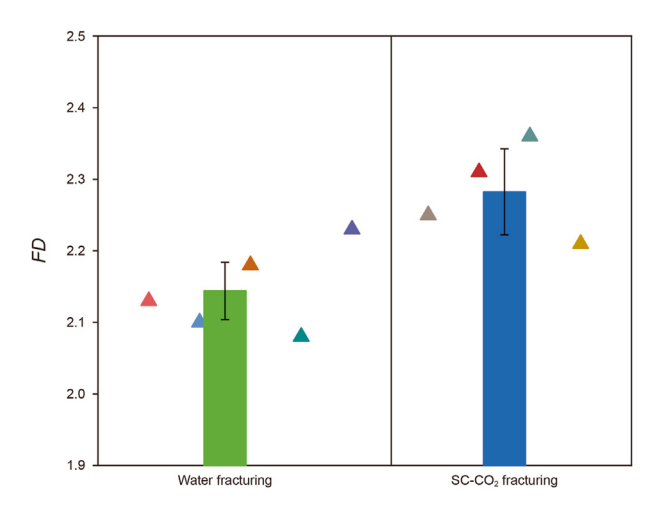


**Fig. 19.** The *FD* of fracture induced by water and SC-CO<sub>2</sub> (the triangle represents the *FD* value of a single fracture, and the bar represents the mean value of *FD*).

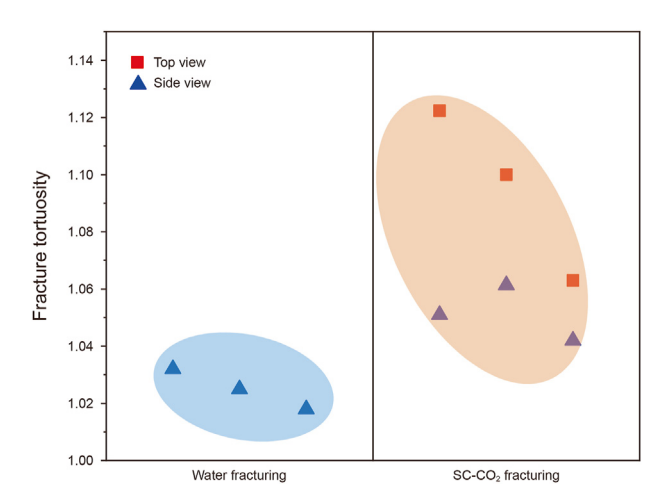
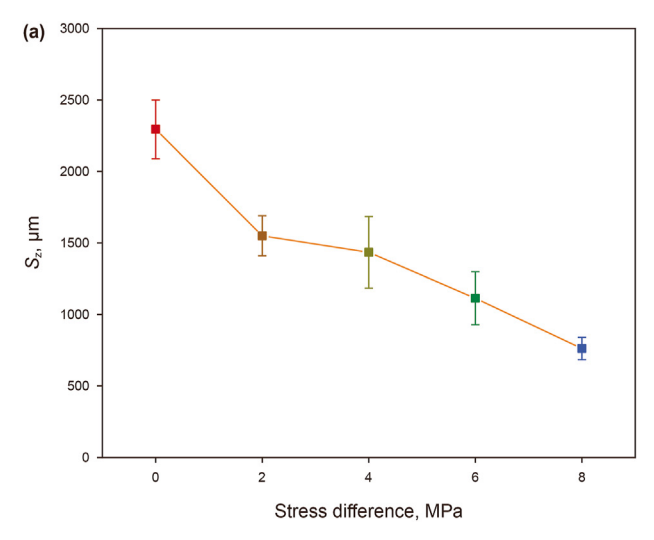


Fig. 20. The tortuosity of fractures induced by water and SC-CO<sub>2</sub>.

H-W equation (Hubbert and Willis, 1957):

$$P_{\rm b} = 3\sigma_{\rm h} - \sigma_{\rm H} + \sigma_{\rm t} - P_{\rm p} \tag{4}$$



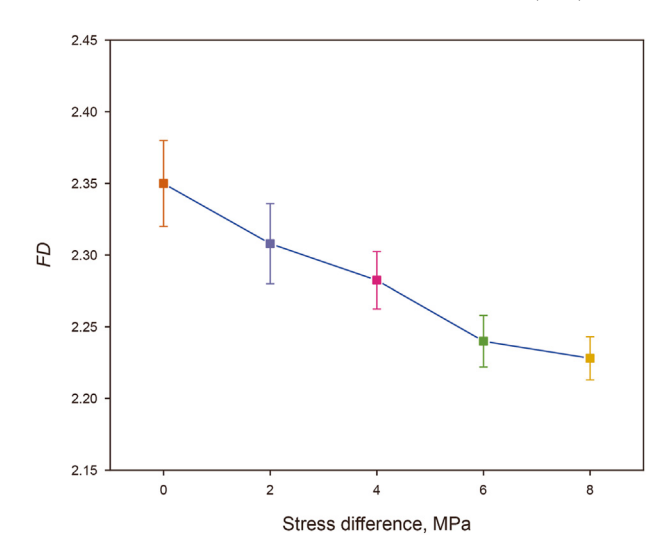


Fig. 22. The FD of fracture induced by SC-CO<sub>2</sub> under different HPSD.

where  $\sigma_t$  is the tensile strength of rock; and  $P_p$  is the pore pressure. If the core sample is treated as an elastic medium with no pore spaces or pore pressure,  $P_b$  can be simplified as

$$P_{\rm b} = 3\sigma_{\rm h} - \sigma_{\rm H} + \sigma_{\rm t} \tag{5}$$

However, if there is natural pore pressure or fluid permeating into rock, the above equation (H—W equation) can be modified as H—F equation (Haimson and Fairhurst, 1967; Detournay and Cheng, 1992):

$$P_{\rm b} = \frac{3\sigma_{\rm h} - \sigma_{\rm H} + \sigma_{\rm t} - 2\eta P_{\rm p}}{2(1-\eta)} \tag{6}$$

where  $\eta = \alpha(1-2v)/(1-v)$  is a function of  $\alpha$  and v. The symbol  $\alpha$  refers to the Biot constant, while v represents the Poisson ratio.

It can be seen from Eqs. (4)–(6) that different stress conditions considered in different fracturing processes will have an impact on the rock's breakdown pressure. The water fracturing process can be approximately analyzed using Eq. (4), while the supercritical CO<sub>2</sub> fracturing process is more in line with Eq. (6). This is because SC-CO<sub>2</sub> has stronger permeability and is more likely to enter the tiny pore spaces of the formation, thus causing changes in pore pressure

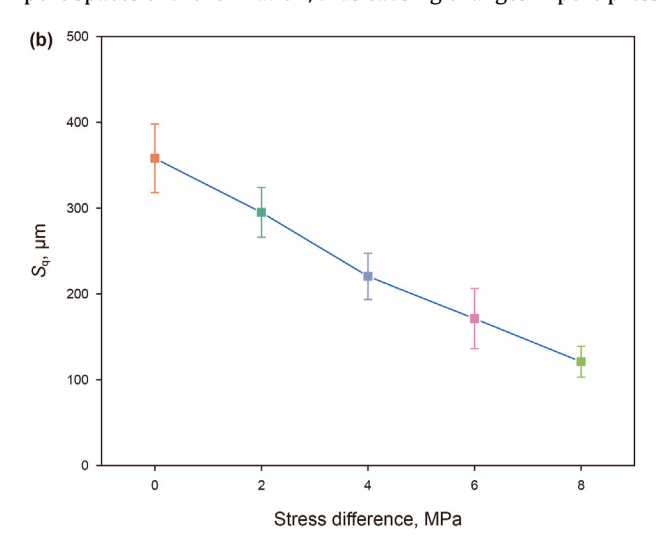


**Fig. 21.** The  $S_z(\mathbf{a})$  and  $S_q(\mathbf{b})$  of fracture surface induced by SC-CO<sub>2</sub> under different HPSD.

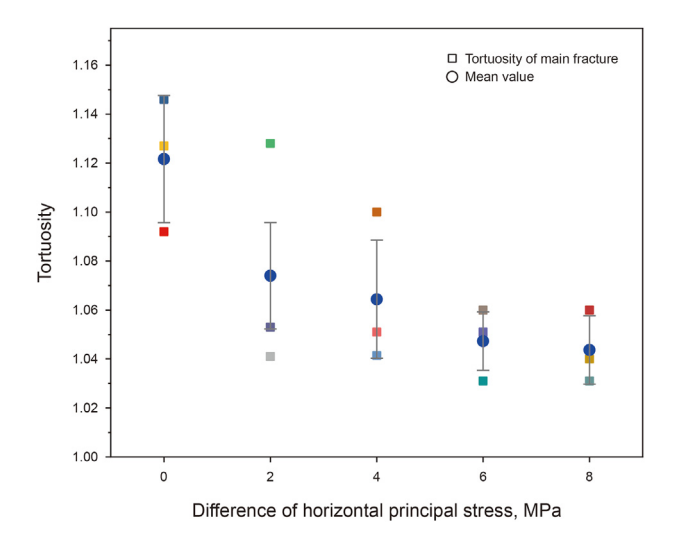


**Fig. 23.** The  $T_0$  of fracture induced by SC-CO<sub>2</sub> under different HPSD.

and resulting in a reduction in the BP. This result can also serve as the reason for the generation of complex fractures induced by SC-CO<sub>2</sub> fracturing.

Based on the spatial 3D distribution and quantitative parameter analysis of fractures, it can be similarly proven that water-based fracturing tends to propagate fractures along original bedding planes. These fractures are fewer in number and exhibit a relatively uniform distribution, indicating a significant influence from the fracturing fluid and original geological structure. The complexity of fractures induced by water-based fluid is similar to previous research findings; however, there are differences in the distribution patterns of the fractures. In Zou's study, the fractures induced by slickwater could intersect with natural bedding planes (Zou et al., 2018). The hydraulic fractures converge with some natural fractures (NFs) and open NFs during the propagation process. This behavior is influenced by the properties of the rock; in this study, the original bonding strength of the bedding planes was relatively low, making it more susceptible to being opened during the fracturing process when exposed to water. In contrast, SC-CO<sub>2</sub> fracturing generates fractures with more complex spatial morphologies and diverse distribution orientations. Quantitative parameters of fractures, such as roughness and tortuosity, exceed those observed in water-based fracturing. It indicates that SC-CO2 fracturing can engender complex fracture patterns characterized by a rougher surface and a more heterogeneous spatial distribution. Some fracture forms do not fully adhere to classical mechanics theories, further demonstrating that SC-CO<sub>2</sub> fracturing can surpass the limitations of geological stress, resulting in complex fractures distributed in multiple directions. These findings affirm the advantages of applying SC-CO<sub>2</sub> fracturing in unconventional low-permeability reservoirs.

Moreover, there are also many differences compared to the results of SC-CO<sub>2</sub> fracturing for shale and coal rock. The most significant differences among these rock samples arise from variations in mineral composition and bonding type, which lead to differences in rock structure and mechanical properties. During the development of shale oil and gas, it is generally recognized that shale is characterized by reservoir tightness, a high content of clay minerals, relatively strong rock brittleness, and the presence of micro-natural fractures. Consequently, it is often easier for complex fractures to form in shale during the fracturing process (Jiang et al., 2018; He et al., 2019). The morphology of these fractures may not necessarily adhere to traditional fracture mechanics theories; they

exhibit diverse distribution directions and readily connect with natural microfractures. In addition, the fracturing process of shale is also greatly affected by in-situ stress conditions, fluid types and natural bedding plane (Li et al., 2016).

Although coal is also relatively dense, it exhibits a rich distribution of bedding and cleat structures, along with a high degree of brittleness. Obtaining natural large-sized coal rock samples is challenging, especially since they tend to break easily during watercooled manual cutting. In experiments, it is common to encase the samples in a layer of cement for stabilization, or different rock bonding simulated interlayers are used to carry out experiments (Wang and Liang, 2019). The induced fractures typically propagate along the natural layering direction and may intersect with NFs, resulting in a favorable degree of fracture development (He et al., 2023). In fact, the research on coal fracturing is a hot spot at present, and the nature of coal determines that this kind of fracturing experiment is more difficult. It is hard to obtain experimental rock samples, and the existing experimental rock samples are small in size and most of them are combined with other lithology or cement, so further exploration is still needed in the future.

# 4.2. Fracture characteristics induced by SC-CO<sub>2</sub> fracturing

Based on the in-situ stress distribution of the target formation, this study investigates the influence of HPSD on fractures induced by SC-CO<sub>2</sub> fracturing. By maintaining the vertical principal stress constant, the study initially analyzed the BP of rocks under different horizontal stress conditions. The results indicate that as the HPSD decreases (with the minimum horizontal principal stress gradually increasing), the BP of the rocks increases accordingly; conversely, the BP decreases as the HPSD increases. Additionally, the presence of abnormal-high stress conditions appears to correlate with a heightened BP in the rock. These findings can be interpreted using classical principles of fracture mechanics. According to these principles, when a rock is subjected to a greater applied stress, the fluid (in this case, SC-CO<sub>2</sub>) must overcome greater strength to induce the rock breakdown. As a result, an increase in the HPSD contributes to a reduction in the BP of the rocks. This result can also be explained by Eqs. (4) or (6). When the maximum principal stress remains constant, the HPSD can be increased by reducing the minimum horizontal principal stress value. It will lead to a decrease in the numerator of the formula, resulting in a slight reduction in the BP value. At the same time, due to the changes in pore pressure caused by the entry of SC-CO<sub>2</sub>, the degree of this reduction may be different. This finding has implications for understanding and optimizing the fracturing process in rock formations under different stress conditions. These findings offer valuable insights into the complex interplay between stress factors and the fracturing behavior under SC-CO<sub>2</sub>, shedding light on potential implications for optimizing fracturing processes in high-stress environments.

The 3D reconstruction results and quantitative parameter analysis of fractures indicate that as the HPSD increases, the spatial distribution of fractures tends to simplify, and the number of fractures gradually decreases. Parameters such as roughness and tortuosity of fractures also decrease gradually. Conversely, as the HPSD decreases, the spatial distribution of fractures becomes more complex, and the propagation directions of fractures become more diverse. Consequently, parameters such as roughness and tortuosity of the formed fractures increase accordingly. These trends are more pronounced under conditions of exceptionally high pressure. It is proposed that a small HPSD, coupled with high fracturing energy, enhances the likelihood of activating discontinuities. This, in turn, leads to the development of a complex fracture pattern, as highlighted in previous research (Zhang et al., 2019). This

observation underscores the intricate interplay between stress conditions and fracturing energy in shaping the fracture morphology within the rock matrix. In some previous studies, stress coefficient  $\kappa$  was introduced to analyze the fracture characteristics of rock. This parameter is defined as  $\kappa = (\sigma_H - \sigma_h)/\sigma_h$ , corresponding to the constant maximum principal stress in this study, the stress coefficient gradually decreases with the increase of the minimum principal stress. The larger the  $\kappa$  value, the more likely the fracture is to propagate along the maximum horizontal stress direction to form the main fracture, thus reducing the complexity of the fracture (Jiang et al., 2019).

This reaffirms the significant influence of in-situ stress on rock fracturing results, with the SC-CO<sub>2</sub> fracturing process often capable of overcoming higher stress conditions. This study's findings provide valuable insights for optimizing rock fracturing design and predicting fracture development.

# 5. Conclusions

To investigate the characteristics of fracture propagation during SC-CO<sub>2</sub> fracturing, a series of true-triaxial fracturing experiments were conducted, involving the comparison of fluid pressure versus time curves between water and SC-CO<sub>2</sub> fracturing, along with the analysis of rock breakdown pressure (BP). Utilizing a 3D reconstruction method for induced fractures, the spatial morphologies and quantitative attributes of fractures were meticulously acquired. Additionally, the influence of in-situ stress on fracture propagation was systematically explored. The key findings can be summarized as follows.

- (1) The water fracturing process exhibits a relatively short duration due to the weak compressibility of the fluid. A transient fluctuation in fluid pressure can be observed, indicating secondary fracture propagation during the fracturing process. The phenomenon of secondary fracture propagation indicates that the size of the rock significantly affects fracturing. Larger volumes may exhibit different fracturing outcomes, this rarely observed in previous smallscale rock samples.
- (2) In contrast, the SC-CO<sub>2</sub> fracturing consumes approximately ten times longer than the water fracturing, with more than half of this duration dedicated to fluid compression. The compressed fluid accumulates and pressurizes at the wellbore bottom, penetrating into the rock matrix. These effects contribute to a notable reduction in rock BP, with SC-CO<sub>2</sub> fracturing capable of reducing BP of rock by nearly 25.1%. This aligns with previous relevant studies, although there are differences in rock sample types and experimental stress conditions, leading to varying degrees of reduction. This result also confirms that SC-CO<sub>2</sub> is more advantageous for implementing fracturing operations in low-permeability reservoirs.
- (3) The macroscopic morphology and quantitative topographical analysis of fractures reveals that fractures induced by water fracturing propagate predominantly along the horizontal bedding direction. Conversely, under equivalent conditions, the fracture morphology induced by SC-CO<sub>2</sub> fracturing exhibits increased complexity. It is indicated that water-based fracturing is more constrained by rock layering and does not strictly adhere to classical fracture mechanics principles. SC-CO<sub>2</sub> fracturing may surpass the constraints of in-situ stress and bedding planes, resulting in more complex fracture patterns.
- (4) As the vertical stress and maximum horizontal principal stress remain constant, an increase in the horizontal

principal stress difference (HPSD) leads to a gradual decrease in BP of rock. As the HPSD escalates from 0 to 8 MPa, the BP of rock experiences a substantial decline of nearly 36%. Moreover, with the increase in HPSD, SC-CO2 fracturing is more inclined to produce a single fracture. Conversely, as the HPSD decreases, SC-CO<sub>2</sub> fracturing exhibits a proclivity for inducing a complex fracture network, characterized by a more diverse array of fracture propagation directions. This observation suggests that the process of fracture propagation is intricately influenced by both the inherent properties of the rock and the in-situ stress conditions. In field applications, smaller differences in in-situ stress tend to result in a more complex and diverse distribution of fractures, whereas larger stress differentials often lead to relatively singular paths of fracture propagation. It is essential to select fracturing fluids and operational conditions based on the specific circumstances.

In general, the use of large-size rock samples ensures sufficient space for fracture propagation, which is crucial for obtaining realistic results that mimic field conditions more closely. Moreover, utilizing real tight sandstone instead of artificial cement rock sample enhances the authenticity of experimental conditions, making the findings more applicable to real geological scenarios. However, a potential limitation is identified in the reliance on the intrusive mode for acquiring fracture attributes, which could impact the accuracy and reliability of the fracture data obtained. Recognizing this limitation, in the following stage, it is essential for further research on fracture propagation characteristics under insitu conditions. In-situ conditions refer to studying the fractures within their natural environment without disturbing the sample. This is a crucial step towards ensuring that the findings are more representative of actual geological conditions. And, related highprecision in-situ fracture acquisition instruments and methods need to be proposed as well.

# **CRediT authorship contribution statement**

**Bing Yang:** Writing — review & editing, Writing — original draft, Methodology, Investigation, Conceptualization. **Hai Huang:** Conceptualization. **Qian-Qian Ren:** Formal analysis. **Hai-Zhu Wang:** Methodology. **Bin Wang:** Supervision. **Jun Ni:** Supervision. **Yong Zheng:** Methodology. **Wen-Tong Zhang:** Data curation.

# **Declaration of competing interest**

The authors declare that they have no known competing financial interests or personal relationships that could have appeared to influence the work reported in this paper.

# Acknowledgements

This paper is funded by the National Natural Scientific Foundation of China (Nos. 52304008, 52404038, 52474043), the China Postdoctoral Science Foundation (No. 2023MD734223), the Key Laboratory of Well Stability and Fluid & Rock Mechanics in Oil and Gas Reservoir of Shaanxi Province (No. 23JS047), the Youth Talent Lifting Program of Xi'an Science and Technology Association (No. 959202413078). And, we will also appreciate the Youth Innovation Team of Shaanxi Universities for their assistance.

# References

Anderson, R.L., Ratcliffe, I., Greenwell, H.C., et al., 2010. Clay swelling—A challenge in the oilfield. Earth Sci. Rev. 98 (3), 201–216. https://doi.org/10.1016/

#### j.earscirev.2009.11.003.

- Bonnet, E., Bour, O., Odling, N.E., et al., 2001. Scaling of fracture systems in geological media. Rev. Geophys. 39 (3), 347–383. https://doi.org/10.1029/1999RG000074.
- Bennour, Z., Ishida, T., Nagaya, Y., et al., 2015. Crack extension in hydraulic fracturing of shale cores using viscous oil, water, and liquid carbon dioxide. Rock Mech. Rock Eng. 48 (4), 1463—1473. https://doi.org/10.1007/s00603-015-0774-2.
- Chen, Y., Nagaya, Y., Ishida, T., 2015. Observations of fractures induced by hydraulic fracturing in anisotropic granite. Rock Mech. Rock Eng. 48 (4), 1455–1461. https://doi.org/10.1007/s00603-015-0727-9.
- Detournay, E.E., Cheng, A.E., 1992. Influence of pressurization rate on the magnitude of the breakdown pressure. In: The 33th US Symposium on Rock Mechanics (USRMS). American Rock Mechanics Association. https://doi.org/10.1016/0148-9062(93)90814-t.
- Dutilleul, P., Han, L., Valladares, F., Messier, C., 2015. Crown traits of coniferous trees and their relation to shade tolerance can differ with leaf type: A biophysical demonstration using computed tomography scanning data. Front. Plant Sci. 6, 172. https://doi.org/10.3389/fpls.2015.00172.
- Falconer, K.J., 2014. Fractal Geometry: Mathematical Foundations and Applications, 3. General & Introductory Mathematics.
- Gupta, A.P., Gupta, A., Langlinais, J., 2005. Feasibility of supercritical carbon dioxide as a drilling fluid for deep underbalanced drilling operation. In: SPE Annual Technical Conference and Exhibition. https://doi.org/10.2118/96992-MS.
- Hubbert, M.K., Willis, D.G., 1957. Mechanics of hydraulic fracturing. Petroleum Transactions of the AIME 210 (1), 153–168. https://doi.org/10.2118/686-G.
- Haimson, B., Fairhurst, C., 1967. Initiation and extension of hydraulic fractures in rocks. SPE J. 7 (3), 310–318. https://doi.org/10.2118/1710-PA.
- He, J.M., Zhang, Y.X., Li, X., Wan, X.L., 2019. Experimental investigation on the fractures induced by hydraulic fracturing using freshwater and supercritical CO<sub>2</sub> in shale under uniaxial stress. Rock Mech. Rock Eng. 52, 3585–3596. https://doi.org/10.1007/s00603-019-01820-w.
- He, W., Lian, H., Liang, W., et al., 2023. Experimental study of supercritical CO<sub>2</sub> fracturing across coal-rock interfaces. Rock Mech. Rock Eng. 56, 57–68. https://doi.org/10.1007/s00603-022-03070-9.
- Inui, S., Ishida, T., Nagaya, Y., et al., 2014. AE monitoring of hydraulic fracturing experiments in granite blocks using supercritical CO<sub>2</sub>, water and viscous oil. In: 48th U.S. Rock Mechanics/Geomechanics Symposium.
- Ishida, T., Aoyagi, K., Niwa, T., et al., 2012. Acoustic emission monitoring of hydraulic fracturing laboratory experiment with supercritical and liquid CO<sub>2</sub>. Geophys. Res. Lett. 39 (16). https://doi.org/10.1029/2012GL052788.
- Ishida, T., Nagaya, Y., Inui, S., et al., 2013. AE monitoring of hydraulic fracturing experiments conducted using CO<sub>2</sub> and water. In: ISRM International Symposium, EUROCK.
- Ishida, T., Chen, Y., Bennour, Z., et al., 2016. Features of CO<sub>2</sub> fracturing deduced from acoustic emission and microscopy in laboratory experiments. J. Geophys. Res. Solid Earth 121 (11), 8080–8098. https://doi.org/10.1002/2016JB013365.
- Jia, C.Z., Zheng, M., Zhang, Y.F., 2012. Unconventional hydrocarbon resources in China and the prospect of exploration and development. Petrol. Explor. Dev. 39 (2), 139–146 (in Chinese).
- Jia, Y.Z., Lu, Y.Y., Elsworth, D., et al., 2018. Surface characteristics and permeability enhancement of shale fractures due to water and supercritical carbon dioxide fracturing. J. Petrol. Sci. Eng. 165, 284–297. https://doi.org/10.1016/ j.petrol.2018.02.018.
- Jia, A.L., Wei, Y.S., Guo, Z., et al., 2022. Development status and prospect of tight sandstone gas in China. Nat. Gas. Ind. 42 (1), 83–92 (in Chinese).
- Jiang, Y.D., Qin, C., Kang, Z., et al., 2018. Experimental study of supercritical CO<sub>2</sub> fracturing on initiation pressure and fracture propagation in shale under different triaxial stress conditions. J. Nat. Gas Sci. Eng. 55, 382–394. https://doi.org/10.1016/j.jngse.2018.04.022.
- Jiang, C.B., Niu, B.W., Yin, G.Z., et al., 2019. CT-based 3D reconstruction of the geometry and propagation of hydraulic fracturing in shale. J. Petrol. Sci. Eng. 179, 899–911. https://doi.org/10.1016/j.petrol.2019.04.103.
- Kolle, J.J., 2000. Coiled-tubing drilling with supercritical carbon dioxide. In: SPE/CIM International Conference on Horizontal Well Technology. https://doi.org/ 10.2118/65534-MS.
- Li, S.H., Zhang, S.C., Ma, X.F., et al., 2019. Hydraulic fractures induced by water-/carbon dioxide-based fluids in tight sandstones. Rock Mech. Rock Eng. 52 (9), 3323–3340. https://doi.org/10.1007/s00603-019-01777-w.
- Li, X., Feng, Z.J., Han, G., et al., 2016. Breakdown pressure and fracture surface morphology of hydraulic fracturing in shale with H<sub>2</sub>O, CO<sub>2</sub> and N<sub>2</sub>. Geomechanics and Geophysics for Geo-Energy and Geo-Resources 2, 63–76. https://doi.org/10.1007/s40948-016-0022-6.
- Liu, F.Y., Ellett, K., Xiao, Y.T., Rupp, J.A., 2013. Assessing the feasibility of CO<sub>2</sub> storage in the New Albany Shale (Devonian—Mississippian) with potential enhanced gas recovery using reservoir simulation. Int. J. Greenh. Gas Control 17, 111–126. https://doi.org/10.1016/j.ijggc.2013.04.018.
- Liu, J., 2021. Hydraulic fracturing technology and application in shale gas wells. Chemical Engineering and Equipment (6), 105–106 (in Chinese).
- Liu, Y.H., Zhang, J.T., Bai, J., et al., 2023. Numerical study of hydraulic fracturing in the sectorial well-factory considering well interference and stress shadowing. Pet. Sci. 20 (6), 3567–3581. https://doi.org/10.1016/j.petsci.2023.05.020.
- Sinal, M.L., Lancaster, G., 1987. Liquid CO<sub>2</sub> fracturing: Advantages and limitations. J. Can. Petrol. Technol. 26 (5). https://doi.org/10.2118/87-05-01.
- Span, R., Wagner, W., 1996. A new equation of state for carbon dioxide covering the fluid region from the triple-point temperature to 1100 K at pressures up to 800 MPa. J. Phys. Chem. Ref. Data 25 (6). https://doi.org/10.1063/1.555991.

Small, M.J., Stern, P.C., Bomberg, E., et al., 2014. Risks and risk governance in unconventional shale gas development. Environ. Sci. Technol. 48 (15), 8289–8297. https://doi.org/10.1021/es502111u.

- Sakmar, S.L., 2011. Shale gas developments in North America: An overview of the regulatory and environmental challenges facing the industry. In: SPE Unconventional Resources Conference/Gas Technology Symposium. https://doi.org/ 10.2118/144279\_MS
- Shafloot, T.A., Kim, T.W., Kovscek, A.R., 2021. Investigating fracture propagation characteristics in shale using sc-CO<sub>2</sub> and water with the aid of X-ray computed tomography. J. Nat. Gas Sci. Eng. 92, 103736. https://doi.org/10.1016/ i.ingse.2020.103736.
- Tang, J.Z., Zhang, M., Guo, X.Y., et al., 2024. Investigation of creep and transport mechanisms of CO<sub>2</sub> fracturing within natural gas hydrates. Energy 300, 131214. https://doi.org/10.1016/j.energy.2024.131214.
- Wang, L., Yao, B.W., Xie, H.J., et al., 2017. CO<sub>2</sub> injection-induced fracturing in naturally fractured shale rocks. Energy 139, 1094–1110. https://doi.org/10.1016/j.energy.2017.08.031.
- Wang, L., Liang, W.G., 2019. Experimental study on fracture initiation and growth in coal using hydraulic fracturing with SC-CO<sub>2</sub> and water. Chin. J. Rock Mech. Eng. 2680–2689. https://doi.org/10.13722/j.cnki.jrme.2018.0253 (in Chinese).
- Wang, H.Z., Shen, Z.H., Li, G.S., 2012. The development and prospect of supercritical carbon dioxide drilling. Petrol. Sci. Technol. 30 (16), 1670–1676. https://doi.org/ 10.1080/10916466.2010.516301.
- Wang, H.Z., Li, G.S., He, Z., et al., 2018. Experimental investigation on abrasive supercritical CO<sub>2</sub> jet perforation. J. CO<sub>2</sub> Util. 28, 59–65. https://doi.org/10.1016/j.jcou.2018.09.018.
- Wang, H.G., Zhou, B., 2022. Progress and prospect of tight sandstone gas well drilling and completion technologies. Nat. Gas. Ind. 42 (1), 159 (in Chinese).
- Xia, J., Wu, X., 2021. Opportunities and challenges of water resources and green development in shale gas development. J. Earth Sci. Environ. 43 (2), 205–214 (in Chinese).
- Yang, B., Wang, H.Z., Shen, Z.H., et al., 2021a. Full-sample X-ray microcomputed tomography analysis of supercritical CO<sub>2</sub> fracturing in tight sandstone: Effect of stress on fracture dynamics. Energy Fuels. 35 (2), 1308–1321. https://doi.org/10.1021/acs.energyfuels.0c03554.
- Yang, B., Wang, H.Z., Wang, B., et al., 2021b. Digital quantification of fracture in full-scale rock using micro-CT images: A fracturing experiment with N<sub>2</sub> and CO<sub>2</sub>.

  J. Petrol. Sci. Eng. 196, 107682. https://doi.org/10.1016/j.petrol.2020.107682.
- Yang, B., Wang, H., Li, G., et al., 2022. Fundamental study and utilization on supercritical CO<sub>2</sub> fracturing developing unconventional resources: Current status, challenge and future perspectives. Pet. Sci. 19 (6), 2757–2780. https://doi.org/10.1016/j.petsci.2022.08.029.
- Yang, B., Wang, H.Z., Wang, B., et al., 2023. Effect of supercritical CO<sub>2</sub>-water/brine-rock interaction on microstructures and mechanical properties of tight sand-stone. Transp. Por. Med. 149 (1), 87–115. https://doi.org/10.1007/s11242-022-01834-z.
- Yang, B., Ren, Q.Q., Huang, H., et al., 2024. Fracture evolution during CO<sub>2</sub> fracturing in unconventional formations: A simulation study using the phase field method. Processes 12 (8), 1682. https://doi.org/10.3390/pr12081682.
- Zang, Y.X., Wang, Q., Wang, H.Z., et al., 2023a. Laboratory visualization of supercritical CO<sub>2</sub> fracturing in tight sandstone using digital image correlation method. Geoenergy Science and Engineering 225, 211556. https://doi.org/ 10.1016/j.geoen.2023.211556.
- Zang, Y.X., Wang, H.Z., Abderrahmane, H.A., et al., 2023b. Optimization design of CO<sub>2</sub> pre-pad energized fracturing for horizontal wells in shale oil reservoirs: A case study of the Ordos Basin. In: SPE Gas & Oil Technology Showcase and Conference. https://doi.org/10.2118/214142-MS.
- Zou, Y.S., Li, N., Ma, X.F., et al., 2018. Experimental study on the growth behavior of supercritical CO<sub>2</sub>-induced fractures in a layered tight sandstone formation. J. Nat. Gas Sci. Eng. 49, 145–156. https://doi.org/10.1016/j.jngse.2017.11.005.
- Zhang, R.X., Hou, B., Han, H., et al., 2019. Experimental investigation on fracture morphology in laminated shale formation by hydraulic fracturing. J. Petrol. Sci. Eng. 177, 442–451. https://doi.org/10.1016/j.petrol.2019.02.056.
- Zhang, Y.X., He, J.M., Li, X., Lin, C., 2019. Experimental study on the supercritical CO<sub>2</sub> fracturing of shale considering anisotropic effects. J. Petrol. Sci. Eng. 173, 932–940. https://doi.org/10.1016/j.petrol.2018.10.092.
- Zhang, Z., Tang, J.Z., Zhang, J.T., et al., 2024. Modeling of scale-dependent perforation geometrical fracture growth in naturally layered media. Eng. Geol. 336, 107499. https://doi.org/10.1016/j.enggeo.2024.107499.
- Zhao, X.Z., Jin, F.M., Liu, X.W., et al., 2022. Numerical study of fracture dynamics in different shale fabric facies by integrating machine learning and 3D lattice method: A case from Cangdong Sag, Bohai Bay basin, China. J. Petrol. Sci. Eng. 218, 110861. https://doi.org/10.1016/j.petrol.2022.110861.
- Zhou, D.W., Zhang, G.Q., Wang, Y.Y., Xing, Y.K., 2018. Experimental investigation on fracture propagation modes in supercritical carbon dioxide fracturing using acoustic emission monitoring. Int. J. Rock. Mech. Min. 110, 111–119. https://doi.org/10.1016/j.ijrmms.2018.07.010.
- Zhou, D.W., Zhang, G.Q., Zhao, P.Y., et al., 2018b. Effects of post-instability induced by supercritical CO<sub>2</sub> phase change on fracture dynamic propagation. J. Petrol. Sci. Eng. 162, 358–366. https://doi.org/10.1016/j.petrol.2017.12.066.
- Zhou, J.P., Hu, N., Xian, X., et al., 2019. Supercritical CO<sub>2</sub> fracking for enhanced shale gas recovery and CO<sub>2</sub> sequestration: Results, status and future challenges. Advances in Geo-Energy Research 3 (2), 207–224. https://doi.org/10.26804/ager.2019.02.10.